3D Bioprinted Skin Co-Culture Model with Air Liquid Interface (ALI) stratification for Investigating Microbiome-Skin Cell Interactions.

by

Giselle Yolanda Díaz González

Bachelor of Science, Instituto Tecnológico y de Estudios Superiores de Monterrey, Mexico,

2020.

A Thesis Submitted in Partial Fulfillment

of the Requirements for the Degree of

MASTER OF APPLIED SCIENCE

in the Department of Mechanical Engineering

We acknowledge and respect the Lək̓ʷəŋən (Songhees and Xʷsepsəm/Esquimalt) Peoples on whose territory the university stands, and the Lək̓ʷəŋən and W̱SÁNEĆ Peoples whose historical relationships with the land continue to this day.

3D Bioprinted Skin Co-Culture Model with Air Liquid Interface (ALI) stratification for Investigating Microbiome-Skin Cell Interactions.

by

Giselle Yolanda Díaz González

Bachelor of Science, Instituto Tecnológico y de Estudios Superiores de Monterrey, Mexico,

2020.

Supervisory Committee

Dr. Stephanie Willerth, Co-supervisor
Department of Mechanical Engineering

Dr. Stephen Tuffs, Co-supervisor and Outside Member
Department of Biochemistry and Microbiology

Dr. Bosco Yu, Departmental Member
Department of Mechanical Engineering

Abstract

Chronic wounds pose a serious and persistent public health challenge, resulting in devastating patient consequences and imposing a substantial economic strain on healthcare systems. Conventional treatments frequently fail because they target only single characteristics of the wound rather than addressing the complex, interconnected cycle where the microbiome and microenvironment play crucial roles in perpetuating inflammation. To develop effective biotherapies, advanced *in vitro* models that accurately replicate the complex skin microenvironment are urgently needed. Existing models, such as two-dimensional (2D) cultures and animal models, lack the necessary physiological complexity, are hindered by species-specific differences, and present ethical concerns.

Three-dimensional (3D) bioprinting has emerged as a powerful alternative, enabling the creation of *in vitro* skin models that more closely mimic human *in vivo* conditions. The primary goal of this work was to investigate the clinical need, design, and verification of a 3D bioprinted stratified skin co-culture model suitable for studying the intricate interactions between the skin microbiome and cutaneous cells. Constructs were generated using extrusion-based bioprinting (EBB) with a high-viscosity, fibrin-based bioink containing co-cultured human keratinocytes (HEKa) and fibroblasts (HDFs), successfully creating a multi-layered structure replicating the epidermis and dermis. Crucially, epidermal stratification was induced through the Air-Liquid Interface (ALI) methodology to replicate the primary air-liquid barrier where bacteria reside and ensure comprehensive host-microbe dynamics.

The functional maturity and interactions between the host-microbiome within the model were validated through biochemical signaling detection of cytokines through Human Cytokine/Chemokine Panel A 48-Plex Discovery Assay®, analyzing conditioned media collected

pre- and post- inoculation with *Staphylococcus epidermidis* (*S. epidermidis*) and *Staphylococcus aureus* (*S. aureus*), the results confirmed a colonization model capable of restoring the cutaneous barrier and maintaining a stable homeostatic environment through active molecular communication.

Furthermore, achieving comprehensive analysis of this full-thickness, high-viscosity hydrogel construct required optimizing bioprocessing techniques. This process involved utilizing cryoslicing methodology, following specific protocols for cryopreservation infiltration using sucrose and optimal cutting temperature (O.C.T) solution, to preserve scaffold integrity and facilitate accurate microscopic evaluation. Optimized staining procedures, including Hematoxylin & Eosin (H&E) for scaffold stratification development, DAPI immunofluorescence staining for structural morphology, Safranin-O for extracellular matrix (ECM) components, and Gram staining for bacterial characterization, were then employed. This comprehensive framework provides a crucial standardization for creating and analyzing complex 3D skin models, offering a valuable, controllable, reproducible *in vitro* platform. Ultimately, this research aims to facilitate the efficient development of novel biotherapies that encompass microbiome homeostasis to effectively and efficiently address chronic wounds.

Table of Contents

List of Figures

List of Tables

List of Abbreviations

DFU: Diabetic Foot Ulcers
3D: Three-dimensional bioprinting
2D: Two-dimensional bioprinting
SC: Stratum Corneum
ECM: Extracellular matrix
UCA: Urocanic acid
NMFs: Natural moisturizing factors
TEWL: Transepidermal water loss
DCs: Dendritic cells.
APCs: Antigen-presenting cells
LCs: Langerhans cells
T_{reg}: T regulatory cells
IL-10: Interlukin-10
IFN-γ: Interferon-gamma
TRM: Tissue-resident memory cells
S. epidermidis: *Staphylococcus epidermidis*
S. aureus: *Staphylococcus aureus*
CoNS: Coagulase-negative staphylococci
AMP: Antimicrobial peptides
Esp: Extracellular serine protease
AIP: Autoinducing peptides
***Arg*:** Accessory gene regulator.
Sph: Sphingomyelinase enzyme
FnbpA: Fibronectin binding proteins A
FnbpB: Fibronectin binding proteins B
IsdA: Iron-regulated surface determinant protein A
PSMs: Phenol-soluble modulins
MRSA: Methicillin-resistant *S. aureus*
PRR: Pattern recognition receptors
O_2: Oxygen
TNF-α : Tumor necrosis factor-α
IL-1β: Interleukin-1β
MMPs: Matrix metalloproteinases
LTA: Lipoteichoic acid
SAgs: Superantigens
HA: Hyaluronic acid
GelMA: Gelatine methacrylate
EBB: Extrusion-based bioprinting
ALI: Air-Liquid interface
O.C.T: Optimal Cutting Temperature
H&E: Hematoxylin & Eosin
GAGs: Glycosaminoglycans
DAPI: 4',6-diamidino-2-phenylindole
DNA: Deoxyribonucleic acid
CO_2: Carbon dioxide
FBS: Fetal Bovine Serum
PBS: Phosphate-buffered saline
EDTA: Trypsin-ethylenediaminetetraacetic acid
HDFs: Human dermal fibroblast
HBSS: Hank's Balanced Salt Solution
DPBS: Dulbecco's Phosphate-Buffered Saline
DMEM: Dulbecco's Modified Eagle Medium
HKGS: Human Keratinocyte Growth Supplement
LSGS: Low Serum Growth Supplement
TBS: Tris-Buffered saline
TrisHCl: Tris hydrochloric acid
Tris base: Tris(hydroxymethyl)aminomethane
NaCl: Sodium Chloride
KCl: Potassium Chloride
DMSO: Dimethyl sulfoxide solution
$CaCl_2$: Calcium chloride
β- GP: β-glycerophosphate
TSA: Tryptic soy agar
TSB: Tryptic soy broth
FI: Fluorescence Intensity
FGF: Fibroblasts growth factor
TGF- α: Transforming Growth Factor - alpha
TNF- α: Tumor Necrosis Factor-alpha
VEGF-A: Vascular Endothelial Growth Factor A
GM-CSF: Granulocyte-macrophage colony-stimulating factor
IL-3: Interlukin-3
IL-10: Interleukin-10
EGF: Epidermal growth factor
CFU: Colony-Forming Unit
PFA: Paraformaldehyde
HD48A: Human Cytokine/Chemokine Panel A 48-Plex Discovery Assay® Array
PC: Phosphocholine
aSMase: Endogenous acid sphingomyelinase
uHF: Upper hair follicle

Acknowledgements

First, I would like to express my deepest gratitude to my supervisor Dr. Willerth that since 2019 provided me with the invaluable opportunity to have a research internship at her laboratory, were I got experience and fascination of the impactful and novel field of 3D bioprinting. From that moment, a seed was planted within me, igniting a passion to continue developing 3D models to optimize preclinical studies in skin biotherapies treatments. As I embarked on my master's degree, her guidance, unconditional support, and belief in me as an individual capable of generating disruptive and novel ideas that could be extended beyond the bench to the market had helped me to become a more well-rounded and complementary graduate student. Furthermore, her efforts in connecting me with the right people and providing opportunities to present my work have significantly fostered my research and allowed me to forge meaningful connections, networking.

I would like to thank my co-supervisor, Dr. Tuffs. He has been an exceptional mentor, that taught me to view every failed result not as a defeat; instead, he skilfully guided me to understand it as part of the process and necessary to leading me closer to the expected outcomes.

To all the members of the Willerth and Tuffs lab who have encouraged and helped me along the way. To Mr. Victor da Silva, Dr. Amanda Orr, Ms. Madeleine Perry, Ms. Silken Tschofen, Ms. Kali Scheck, Mr. Dmitri Karaman and all the co-op and MITACS students for being part of and helping me along this journey. It's been a privilege to collaborate, learning, teaching, optimizing process, and making new discoveries together.

Dedication

Para mis padres, que la herencia que me dejaron fue la oportunidad de acceder a la educación, otorgándome el privilegio de amar el aprendizaje.

A mi amado, que me ha enseñado el “cómo”, más que el “porqué”.

Y a la ciencia, que me concientizó que el conocimiento es dudar; que hay que hacer, experimentar y fracasar para saber, dejándome el legado de que, para entender genuinamente y desarrollarme, hay que poner en práctica lo aprendido y lo sabré.

General notes and article-by thesis statement

This thesis is to be submitted as an *article-by-thesis* format.

The following sections, figures, and tables of **Chapter 1: Introduction and Chapter 2: Material and Methods** have been extracted and/or minimally adapted from two *published* review articles of which I am first author (with consent from all co-authors). The content of the reviews and research paper were adapted into a thesis-format to comply with the guidelines provided by the Faculty of Graduate studies at the University of Victoria.

The first: **Díaz GY,** Da Silva VA, Kalantarnia F, Scheck K, Tschofen SA, Tuffs SW, Willerth SM. Using Three-Dimensional Bioprinting to Generate Realistic Models of Wound Healing. *Advances in wound care*, 10.1089/wound.2024.0138. 5 Mar. 2025, doi:10.1089/wound.2024.0138

The second: **Díaz GY**, Perry MA, Cárdenas LS, Da Silva VA, Scheck K, Tschofen SA, Tuffs SW, Willerth SM. Protocol for 3D Bioprinting a Co-culture Skin Model Using a Natural Fibrin-Based Bioink as an Infection Model. *Bio-protocol* vol. 15,14 e5380. 20 Jul. 2025, doi:10.21769/BioProtoc.5380

In both above publications, I have significantly contributed to the literature review, article conceptualization, figure creation, writing, and reviewing-totalling more than 80% of the overall contribution.

CHAPTER 1- INTRODUCTION

1.1 Skin: A complex and vulnerable organ.

The skin is the largest organ on the human body, serving as a dynamic interface between our internal organs and the external environment (Derman et al., 2024). Its multifaceted functions encompass mechanical protection, preventing water loss, and thermoregulation. It also plays key roles in sensing external stimuli and regulating the immune response (Peña et al., 2024). However, because it is the most exposed organ, the skin is inherently vulnerable to damage. In most cases, the wound healing process occurs through a coordinated series of phases, which remodel the tissue and lead to a complete resolution (Shai et al., 2005). Nonetheless, when a wound is inappropriately managed, it can lead to a cycle of persistent inflammation, increased susceptibility to infections, and inhibited healing; what could have been treated as an acute wound has developed into a chronic wound (Keast et al., 2012).

These non-healing, or chronic wounds (including diabetic foot ulcers (DFU), infected lacerations, burns, and pilonidal or perianal abscesses) are a serious public health problem that have devastating quality life consequences for patients and impose a substantial economic strain to the health-care systems (Dreifke et al., 2015). According to Wounds Canada (2025) up to 25% of the nearly 5.7 million Canadians living with diabetes will develop a DFU in their lifetime (Gray, 2025). Collectively, the health-care costs associated with DFU amounts to $750 million annually (Kuhnke et al., 2024).

Presently, the care for chronic wounds varies depending on the wound etiology, size, and the progression of healing, but usually includes debridement of callused areas, wound dressings, footwear or clothes adaptation/offloading and antifungal, antimicrobials therapy (Pérez-Panero et al., 2019). Despite these best clinical practices, conventional treatments fail to effectively promote the closure of hard-to heal chronic wounds. Their failure lies in that they target a single characteristic of the wound rather than treating it as a complex, interconnected cycle where the microbiome and microenvironment play crucial roles in either promoting healing or perpetuating inflammation (Mamun et al., 2024). Therefore, there is an urgent need to develop new biotherapeutics that address this intricate interplay to create comprehensive solutions for chronic wound healing.

Even so, to develop new wound healing therapies, advanced *in vitro* models that accurately replicate the complex skin microenvironment and microbiome are needed. These models would not only allow for high throughput testing of potential therapeutics in a realistic environment but also could be used to gain further insight into the complex mechanisms that prevent chronic wounds from healing. Three-dimensional (3D) bioprinting has emerged as a powerful alternative, enabling the creation of *in vitro* skin models that more closely mimic human *in vivo* conditions.

Using bioinks, biocompatible hydrogels containing living cells, 3D bioprinting allows for precise spatial organization and the formation of tissue-like structures, including multi-layered constructs that replicate the dermis and epidermis (Díaz et al., 2025). This approach overcomes the lack of physiological complexity, species-specific differences, and ethical concerns that are inherent limitations of two-dimensional (2D) and animal models (Kamel et al., 2024).

This thesis framework will investigate the clinical need, design, and verification of a colonized 3D human skin model specifically developed to study the intricate interactions between the skin

microbiota and the cutaneous skin cells. By providing a valuable tool for understanding host-microbe dynamics and skin infections, this research aims to facilitate the development of novel therapies that encompass the complex interplay of various factors within the wound microenvironment that can either impede or promote the healing of chronic injuries.

1.2 Anatomy of Human Skin

The epidermis lacks a vascular system, as it has no blood vessels, and is primarily composed by keratinocytes that undergo a tightly controlled terminal differentiation to form the stratum corneum (SC) (Dwivedi et al., 2019). The epidermis is subdivided into five main layers: the stratum corneum, stratum lucidum, stratum granulosum, stratum spinosum and stratum basale (Yousef et al., 2025).

The outermost layer of the epidermis, the stratum corneum, is known as the structural epidermal barrier. It is conceptualized as a “bricks-and-mortar” structure, composed of terminally differentiated keratinocytes (corneocytes) that "roll over" from the stratum granulosum (Stefanovic et al., 2024). The anuclear corneocytes, which act as the "bricks," are held together by corneodesmosomes and are embedded in a "mortar" of lipid-rich extracellular matrix (ECM), including free fatty acids, cholesterol, and ceramides. During keratinocyte differentiation, filaggrin, a histidine-rich protein, is degraded into its constituent breakdown products, such as free amino acids and urocanic acid (UCA). These water-soluble, low-molecular-weight molecules are key components of the skin’s natural moisturizing factors (NMFs) and contribute to the regulation of skin pH (being acidic) and transepidermal water loss (TEWL) (Figure 1) (Kezic et al., 2011). Furthermore, the skin's resident microbiota is maintained on the upper half of the stratum corneum by keeping the homeostatic balance relationship fostered by a coordinated interplay of

immunomodulatory functions from both the humoral and adaptive immune systems in the skin (Krieken et al., 2016).

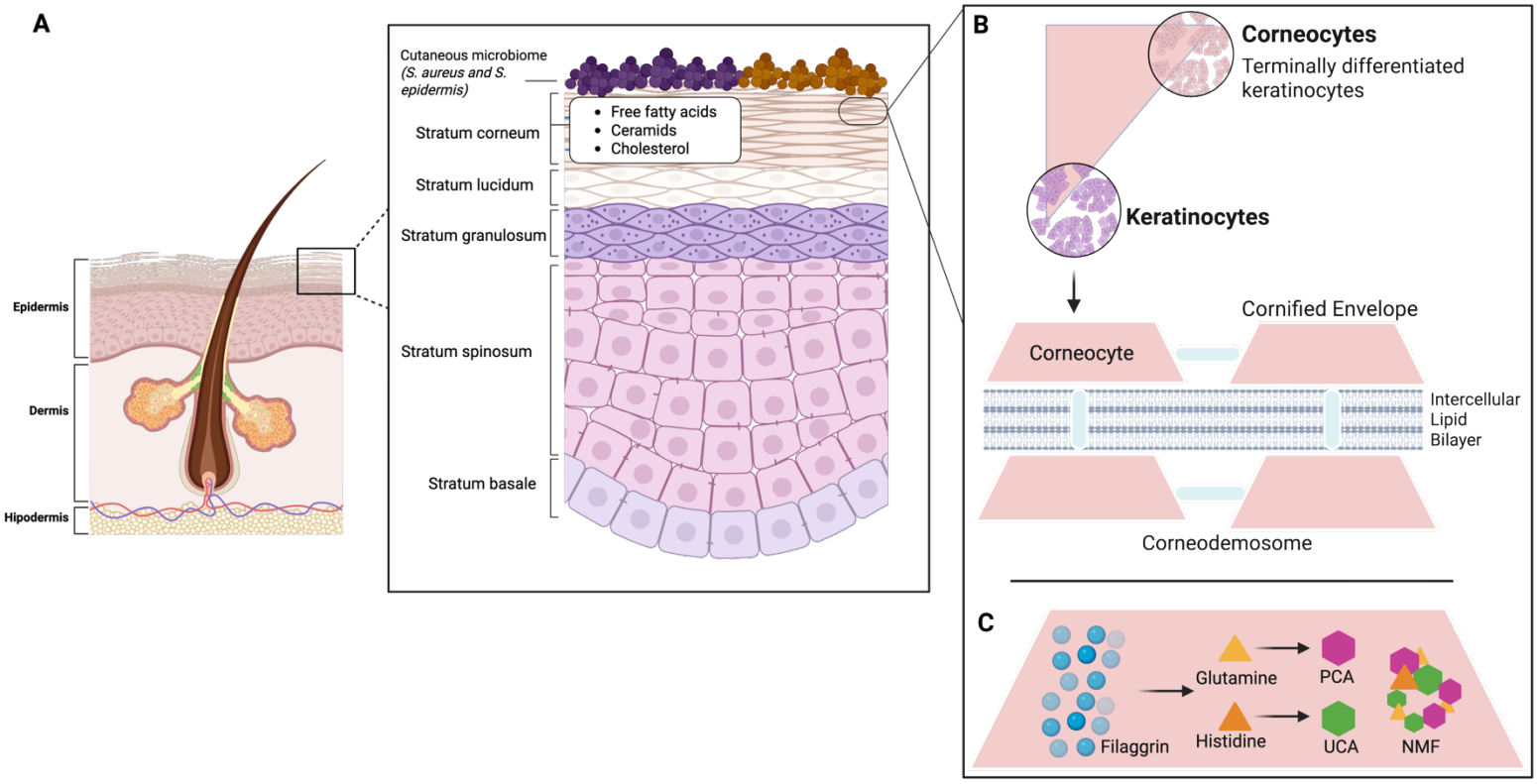

Figure 1. Structural and biochemical organization of the human skin barrier. (A) The skin consists of three primary layers, the epidermis, dermis, and hypodermis, with the epidermis stratified into the stratum basale, spinosum, granulosum, lucidum, and corneum. The upper half of the stratum corneum (SC) hosts the cutaneous microbiota, including *Staphylococcus aureus* (*S. aureus*) and *Staphylococcus epidermidis* (*S. epidermidis*), and is enriched with a lipid matrix of free fatty acids, ceramides, and cholesterol. **(B)** The SC it is conceptualized a "brick and mortar" structure, composed of terminally differentiated keratinocytes, called corneocytes that “roll over” from the stratum granulosum. The anuclear corneocytes, which act as the “bricks”, are held together by corenodesmosomes and are embedded in a “mortat” of lipid-rich extracellular matrix (ECM), including fatty acids, cholesterol, and ceramids. **(C)** During cellular differentiation, the protein filaggrin is proteolytically processed into amino acids such as glutamine and histidine, which are further metabolized into pyrrolidone carboxylic acid (PCA) and urocanic acid (UCA), respectively. These water-soluble, low-molecular-weight molecules are major constituents of the Natural Moisturizing Factor (NMF), which is essential for regulating skin hydration, maintaining surface pH, and controlling transepidermal water loss (TEWL) while exerting key immunomodulatory effects. Created in BioRender. Tuffs, S. (2026) https://BioRender.com/undefined

The dermis that underlies the epidermis is divided into two distinct layers: the papillary dermis and the reticular dermis. The papillary dermis is the superficial layer, situated deep to the epidermis, and is composed of highly vascular, loose connective tissue. In contrast, the reticular layer is the deeper and thicker layer, forming the bulk of the dermis with its dense connective tissue (Brown et al., 2025). Structurally, the dermis is fundamentally supported by collagen (types I and III), while the presence of elastic fibers, which are composed of elastin and fibrillin microfibrils, allows the skin to stretch and recoil (Prost-squarcioni et al., 2008).

Fibroblasts are the principal cells of the dermis, responsible for synthesizing collagen, elastic and reticular fibers, and the extracellular matrix (Lopez-Ojeda et al., 2025). Additionally, the dermis contains mast cells, which are resident inflammatory cells that secrete vasoactive and proinflammatory mediators. These mediators play an important role in inflammatory reactions, collagen remodelling, allergic responses and wound healing (Wilgus et al., 2014).

1.3 Skin Microbiome

The skin is naturally colonized by transient, temporarily resident, and permanently resident bacterial species, including *Staphylococci*, *Micrococcus spp*., and *Coryneform* bacteria. These microorganisms exist in either a mutualistic and/or competitive relationship with each other (microbe-microbe) and the host (Zhang et al., 2024). The skin's surface comprises diverse microenvironments with distinct pH, moisture, temperature, and topography that regulate the delicate balance between the host and its resident microbes. Through immune tolerance, the skin can distinguish between harmless commensal microorganisms and harmful pathogens (Díaz et al., 2025).

The skin's immune defence is supported by specialized cells. Dendritic cells (DCs) are efficient antigen-presenting cells (APCs) that migrate to draining lymph nodes to interact with the

naïve T cells ($CD4^+$ and $CD8^+$) to induce an immune response (Chudnovskiy et al., 2019). Within the epidermis, Langerhans cells (LCs), serve as resident innate immune cells that act as DC; upon activation, these cells migrate to skin-draining lymph nodes, where they play the role of APCs (Neagu et al., 2022). Conversely, the dermis has dermal interstitial DCs that promote effector T cell responses (Klechevsky et al., 2008). CD4+T regulatory cells (T_{reg}) frequently found in the dermis, play a central role in the process of immune regulation and tolerance against the microbiome of the skin, because they either can secrete regulatory cytokines as Interlukin-10 (IL-10) for anti-inflammatory regulation functions or differentiate into T helper cells releasing pro-inflammatory cytokines as interferon-gamma (IFN-γ) which activates macrophages to phagocytose pathogens (Round et al, 2010; Zheng, 2013). CD8+ tissue-resident memory cells (TRM) are mainly located in the epidermis and provide an immediate barrier against re-infection by releasing cytokines and cytotoxic components (Funch et al., 2022).

Homeostasis between the host and the microbes is maintained through a delicate symbiosis. In this interaction, commensal bacteria, such as *Staphylococcus epidermidis* (*S. epidermidis),* actively inhibit the growth and toxicity of pathogenic microorganisms like *Staphylococcus aureus (S. aureus).* In response, the host recognizes and tolerates these beneficial microorganisms, allowing their growth (Lee et al., 2022). This represents a mutually beneficial interaction where the microorganisms obtain essential nutrients and a habitat, and in return, they facilitate the maintenance of the barrier integrity and functional capacity of the skin barrier (Volksdorf et al., 2018).

1.3.1. *Staphylococcus epidermidis*

S. epidermidis is a Gram-positive, non-motile and facultative anaerobic bacterium. Among the staphylococci, it can be assigned to the group of coagulase-negative staphylococci (CoNS) (Chabi et al., 2019). By the expression of several adhesion molecules, cell wall-anchored proteins and induction of commensal-specific regulatory T (T_{reg}) cells, the bacteria can live as a commensal on the stratum corneum (Ali et al., 2017; Conwill et al., 2022). *S. epidermidis* have several beneficial effects for the host since they modulate the innate immune system by stimulating the release of antimicrobial peptides (AMP) by the keratinocytes, such as β-defensins and cathelicidin, which undermine pathogenic *S. aures* biofilms. Furthermore, *S. epidermidis* secretes extracellular serine protease (Esp), which inhibits *S. aureus* colonization by degrading proteins essential for adhesion and biofilm formation (Iwase et al., 2010). Moreover, *S. epidermidis* autoinducing peptides (AIP) has been proven to inhibit the accessory gene regulator (*arg*) system, such as *agr*-1_{Sa} to *agr*-3_{Sa}, suppressing the expression of key *S. aureus* virulence factors (Nair et al., 2014).

Beyond its role in microbial defence, *S. epidermidis* has been shown to play a crucial role in keeping the physical integrity of the skin barrier (Lee et al., 2022). This is achieved by secreting sphingomyelinase enzyme (Sph), which increase skin ceramide levels, thereby preventing water loss and maintaining the lipid structure of the epidermis (Figure 2) (Zheng et al., 2022).

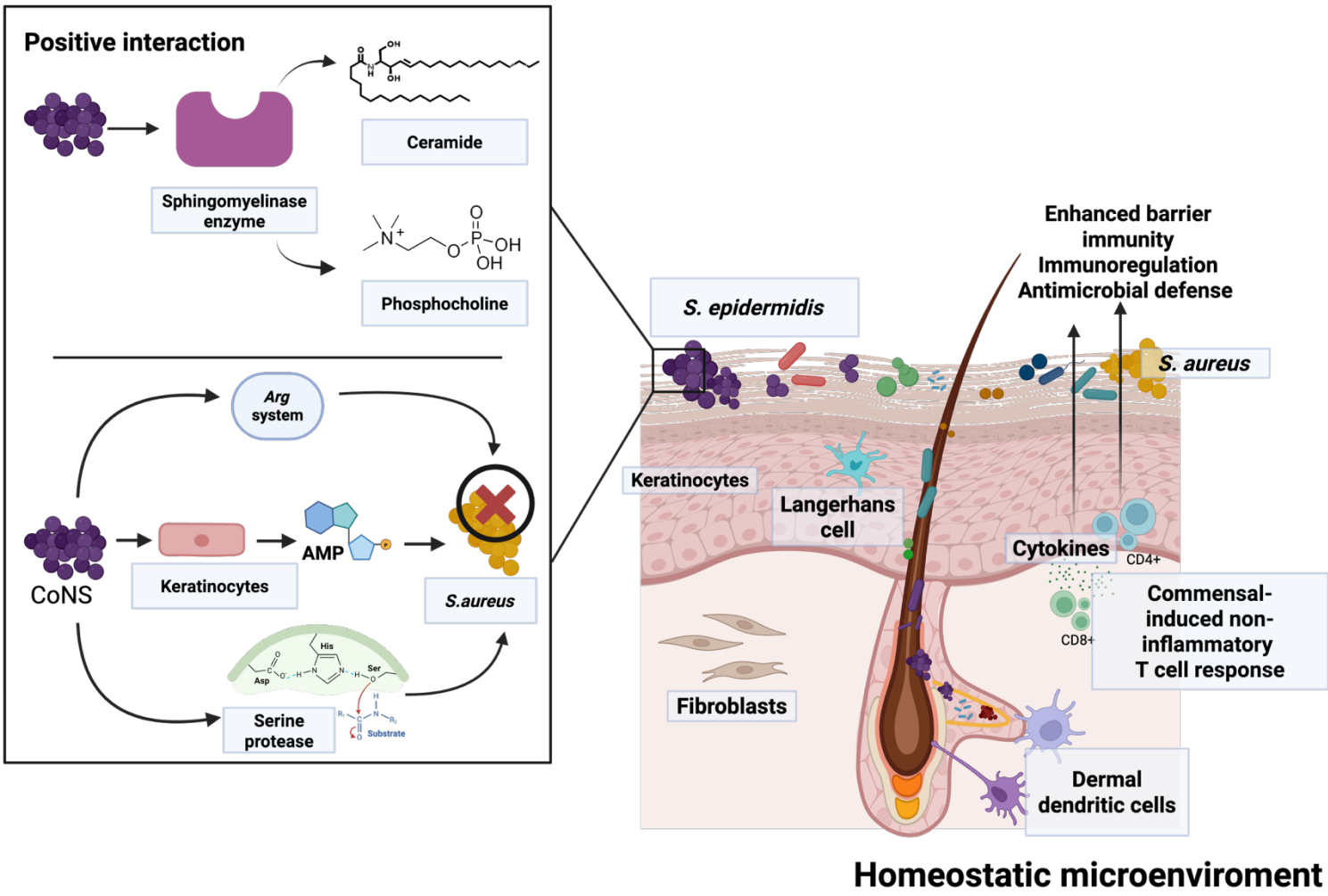

Figure 2. Mechanisms of microbial homeostasis and immune regulation in the skin. The skin acts as a specialized environment where distinct chemical and physical factors, including pH, moisture, and temperature, regulate the symbiotic balance between the host and resident microorganisms. Homeostasis is maintained through a mutually beneficial relationship where commensal bacteria, particularly coagulase-negative staphylococci (CoNS) such as *Staphylococcus epidermidis* (*S. epidermidis*), actively inhibit the growth and toxicity of pathogens like *Staphylococcus aureus* (*S. aureus*). This inhibition is mediated by the secretion of extracellular serine protease (Esp), which degrades proteins essential for *S. aureus* biofilm formation, and autoinducing peptides (AIP) that suppress the *S. aureus* accessory gene regulator (*agr*) system to reduce virulence. Beyond microbial defense, *S. epidermidis* supports the physical integrity of the skin barrier by secreting the sphingomyelinase enzyme, which increases ceramide levels to prevent water loss and maintain epidermal lipid structure. Simultaneously, the host's immune system facilitates this symbiosis via specialized cells: Langerhans cells in the epidermis and dermal dendritic cells act as antigen-presenting cells to induce targeted immune responses. This network includes CD4+ T regulatory cells (T_{reg}) that promote immune tolerance through anti-inflammatory cytokines like IL-10, and CD8+ tissue-resident memory cells (TRM) that provide an immediate defense against re-infection, ensuring the skin effectively distinguishes between harmless commensals and harmful pathogens. Created in BioRender. Tuffs, S. (2026) https://BioRender.com/undefined

1.3.2 *Staphylococcus aureus*

S. aureus is a Gram-positive, non-motile, and facultative anaerobic bacterium, classified among the coagulase-positive staphylococci (Foster et al., 1996). This organism is equipped with several surface molecules, such as clumping factors A and B, fibronectin binding proteins A and B (FnbpA and B), and iron-regulated surface determinant protein A (IsdA), which facilitate its adherence to the stratum corneum (Zhang et al., 2024). Acting as an opportunistic pathogen, *S. aureus* expresses various toxin factors and proteases when a barrier disruption is present. These agents are crucial in damaging the skin barrier, promoting deeper bacterial penetration, and releasing phenol-soluble modulins (PSMs) that stimulate cytokine production, ultimately leading to a state of persistent skin inflammation (Patra et al., 2018). Consequently, though *S. aureus* is part of the normal skin microbiota, it is also a major pathogen responsible for human diseases, ranging from uncomplicated skin and soft tissue infections to life-threating pneumonia and septicemia (Le et al., 2025). This capacity for disease is further demonstrated by the fact that 37% of surgical site infections are provoked by *S. aureus* (Pal et al., 2019). Furthermore, because of the high rate of antimicrobial resistance among *S. aureus* clinical isolates, such as methicillin-resistant *S. aureus* (MRSA), limits the clinical effectiveness of current therapeutics, leading to higher mortality and morbidity rates and increasing healthcare-associated costs (Fukuda et al., 2020). For example, in DFU patients 40-60% of *S. aureus* infections persistently recur even after the infection appears cleared in the early stages of the treatment, and causing a mortality rate of 60% of the patients that presented an infection (Liu et al., 2024).

1.3.3 Dysbiosis

As mentioned before, the host and the skin microbiota co-interact in homeostasis, collaborating to preserve the skin barrier function, modulating the adaptive immune response, improve barrier immunity, and prevent the entry of pathogens (Zhang et al., 2024). However, when a disruption, such as a wound, occurs, the skin microbiota can disrupt this stage of homeostasis, a state known as dysbiosis. This alters the ecological interaction between microorganisms and the host, triggering skin inflammation (Zhang et al., 2022). A dysbiotic environment can allow the invasion of pathogenic bacteria such as *S. aureus.* This can further amplify inflammation starting with the pattern recognition receptors (PRR) on macrophages triggering the secretions of pro-inflammatory cytokines, which strongly induce the release of AMPs, leading to the differentiation of T lymphocytes, which further stimulates the release of inflammatory mediators that stimulate the formation of chemokines and release more AMPs which creates a "vicious cycle" of inflammation (Šuler Baglama, et al., 2022).

1.4 Wound healing

Healing a skin wound requires extraordinary mechanisms of cellular functions that are distinctive in nature. The repair process consists of four stages: homeostasis, inflammation, proliferation, and remodeling. At the beginning of the healing process, a blood-filled wound is first closed by a fibrin coagulum that acts as a scaffold for cell infiltration (Shai et al., 2005). Second, inflammation occurs simultaneously as neutrophils infiltrate the wound site to initiate the inflammatory response, where they are replaced by monocytes that differentiate into macrophages. Proliferation begins 2–10 days after the lesion was made and consists of "rebuilding" involving re-epithelialization, angiogenesis, collagen synthesis, and extracellular matrix deposition (Kathawala et al., 2019). Angiogenesis is an important event during healing process where new

capillaries are formed from existing blood vessels (Schultz et al., 2011). Specifically, endothelial cells that constitute the inner cellular lining of the blood vessels (arteries, veins, and capillaries) form new capillaries, which is essential for bringing oxygen (O_2) and nutrients to the growing tissue and removing waste products (Félétou, 2011). Following this, the formation of granulation tissue allows re-epithelialization, where the keratinocytes roll over from the basal layer to restore the physiological features of the multilayered epithelial tissue (Usui et al., 2008).

1.4.1 Chronic Injuries

As previously mentioned, acute wound healing follows the normal physiological repair process, whereas chronic wounds are marked by a persistent inflammation phase due to persistent immune dysregulation, which delays healing (Kathawala et al., 2019). The microenvironment of a chronic wound is characterized by high quantities of proinflammatory macrophages, overexpression of inflammatory mediators such as tumor necrosis factor- α (TNF- α) and interleukin-1β (IL-1β), and increased activity of matrix metalloproteinases (MMPs), namely MMP-2 and MMP-9, which degrade the ECM to allow immune cell infiltration but prevent the commencement of the proliferative stage of healing (Raziyeva et al., 2021).

This failure to heal is initiated by a chemical shift in the skin microenvironment. While the normal skin surface is acidic, the exposure of internal tissue and interstitial fluid (with a normal pH of ~7.40) causes the wound area to become alkaline (pH 7.42−8.90). This shift to an alkaline pH affects oxygen production, interfering with fibroblast growth and collagen synthesis during the healing process (Sim et al., 2022). Any disruption in oxygen tension directly affects the proliferation and migration behaviour of these cells, further impeding wound healing (Schreml et al., 2010).

Furthermore, the loss of the hostile acidic microenvironment and the shift toward alkalinity pH, provides ideal circumstances for opportunistic pathogenic bacteria, such as *S. aureus,* to thrive and invade (Lee et al, 2022). The opportunistic bacteria then actively impair the epidermal barrier by secreting toxins (alpha toxin), proteases and Lipoteichoic Acid (LTA) cell wall product that dissolve the SC and inhibit the expression of epidermal barrier proteins (fibroin and loricrin), leading to an impaired skin barrier function. With both physical and chemical barriers disrupted, the opportunistic bacteria further promote a dysregulated immune system action, releasing Superantigens (SAgs) that increase the activation of T cells, leading to an overproduction of cytokines provoking a persistent wound in an inflammatory phase (Figure 3) (Zhang et al., 2024).

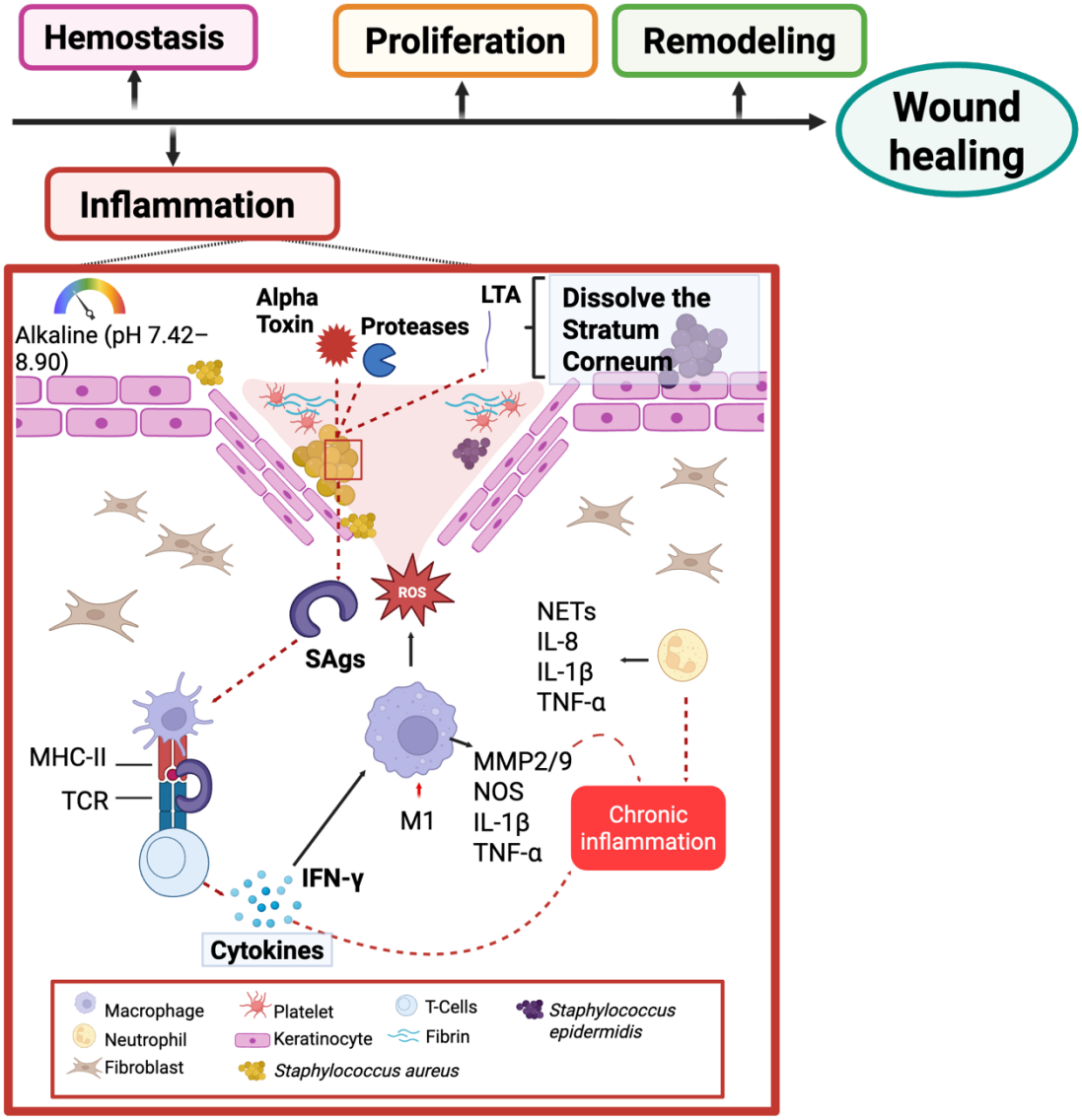

Figure 3. Dysbiotic microenvironment and mechanisms of persistent inflammation in chronic wounds. Wound healing typically progresses through four orchestrated stages: hemostasis, inflammation, proliferation, and remodeling. In chronic injuries, this process is interrupted by a persistent inflammatory phase initiated by a chemical shift from the skin's natural acidity to an alkaline microenvironment (pH 7.42–8.90). This alkalinity interferes with fibroblast growth and collagen synthesis while providing an ideal habitat for opportunistic pathogens like *Staphylococcus aureus* (*S. aureus*) to thrive. These bacteria further impair the barrier by secreting alpha-toxins, proteases, and lipoteichoic acid (LTA), which dissolve the stratum corneum (SC) and inhibit the expression of essential barrier proteins like loricrin. This structural breakdown allows the infiltration of superantigens (SAgs) that over-activate T cells, leading to a cytokine storm, including tumor necrosis factor- α (TNF- α) and interleukin-1β (IL-1β) and IL-8, and the recruitment of proinflammatory M1 macrophages. These macrophages release reactive oxygen species (ROS) and matrix metalloproteinases (MMP-2/9) that degrade the extracellular matrix, preventing the transition to the proliferative stage and trapping the tissue in a state of chronic inflammation. Created in BioRender. Tuffs, S. (2026) https://BioRender.com/undefined

1.4.2 Transition to Treatment Limitations

Despite decades of extensive research on chronic wounds, treatments still rely on traditional approaches like autografts, allografts, and xenografts. These methods are not the optimal methodologies for addressing the complex process of a non-healing wound, as they focus more on managing the injury than on fully restoring tissue integrity (Gao et al., 2021). Therefore, there is an urgent need to develop new methods capable of understanding and incorporating the restoration of microbiome homeostasis for managing microorganism proliferation, pH recuperation, and inflammation control.

However, the existing approaches used to design more effective clinical therapies for chronic wounds mostly rely on two-dimensional cell cultures and animal models. These models have significant limitations: 2D cultures lack physiological complexity, while animal models are hindered by species-specific differences and ethical concerns (Kamel et al., 2024).

For this reason, three-dimensional bioprinting models have emerged as a powerful alternative. This technology enables the creation of *in vitro* skin models that more closely mimic human *in vivo* conditions. Using bioinks, biocompatible hydrogels containing living cells, 3D bioprinting allows for precise spatial organization and the formation of tissue-like structures, including multi-layered constructs that replicate the dermis and epidermis (Tripathi et al., 2023). These models support cell proliferation, differentiation, and physiologically accurate cell interactions, making them ideal platforms for studying bacterial infections and host immune responses in a chronic wound environment (Derr et al., 2019). This represents a crucial step toward developing more effective and sustainable biotherapies for treating non-healing wounds (Edmondson et al., 2014; Heinrich et al., 2019)

1.5 3D Bioprinting skin models

The complex structural configuration of human skin involves the dermal-epidermal junction, which not only provides structural support and a protective barrier, but also actively engages in cellular signalling, metabolic processes, and the nervous, adaptive, and innate immune systems (Rielland et al., 2025). Furthermore, it enables the definition of a microenvironment that allows for the existence of the microbiome. The complexity arising from these multifaceted functions amplifies the challenge to recreate a full-thickness skin model.

3D bioprinting is focused on overcoming these challenges by allowing the manipulation of live cells to be bioprinted in combination with biomaterials. This process uses precise spatial arrangements, which permits the creation of the intricate architecture of the skin, complete with its distinct layers (Varpe et al., 2025). Consequently, the bioink formulation and the chosen 3D bioprinting technique play a critical, interconnected role in developing an efficient scaffold that provides the necessary supporting microenvironment for the skin cells to proliferate, migrate, differentiate, and mature (Weng et al., 2021).

1.5.1 Bioink formulation

To achieve viable models, the biomaterials used as bioinks for skin bioprinting must meet several crucial criteria. They should be printable, degradable, possess sufficient mechanical properties, and be biocompatible with immobilized cells (Rossi et al., 2024). Most importantly, they must exhibit suitable rheological properties to be printable and crosslinked within an efficient time frame. This is essential to avoid negatively affecting the structure of the scaffold and the printed cells (Xu et al., 2022). Such a bioink material should support and preferably enhance cell viability, distribution/migration, proliferation, differentiation and formation of appropriate tissue (Kim, 2023).

Hydrogels-based bioinks are commonly used for skin regeneration and wound healing procedures, but also to create 3D biomimetic microenvironments, because they are highly suitable for recapitulating *in vivo* cellular activities (Aydin et al., 2020). A key feature is their remarkable capacity to retain significant amounts of water, without losing structural integrity, due to hydrophilic components in their polymer structure. This unique attribute of hydrogels highlights their suitability for replicating ECM properties and promoting tissue regeneration (Díaz et al., 2025).

The ECM is composed of a dynamic, three-dimensional arrangement of polysaccharides and natural polymers (collagen, elastin, fibrinogen), which serves as the major structural framework for the skin. Furthermore, the ECM acts as a reservoir and mediator for growth factors and signalling molecules. This allows for efficient communication that is inherently bidirectional: "outside-in" signalling occurs across the cell membrane to the nucleus, providing specific cellular instructions, while "inside-out" signalling allows internal cellular changes to alter the activity of surface receptors (Sell et al., 2010). This vital communication is crucial for processes like cell adhesion, proliferation, and differentiation, as well as for ECM alteration needed for cell migration through the matrix (Pfisterer et al., 2021). The importance of replicating these ECM-cell interactions in bioinks is paramount because this complex signalling network is what allows cells to adapt to shifting microenvironments and efficiently coordinate all restorative actions necessary to reconstitute the wound area. These ECM-mimicking hydrogels may be either natural such as alginate, hyaluronic acid (HA), fibrin, gelatin and collagen or synthetic such as gelatine methacrylate (GelMA) (Wang et al., 2017).

1.5.2 3D bioprinting techniques

The choice of printing method is governed by the bioink's properties, where a high viscosity bioink is essential for maintaining structural integrity, preventing cell sedimentation, and ensuring uniform cell distribution (Chen et al., 2023). However, the requirement for higher viscosity necessitates greater pressure during printing, which increases shear stress at the nozzle tip. This rise in shear stress can reduce cell viability and negatively affect protein signalling and cell phenotype maturation (Stepanovska et al., 2021). Extrusion-based bioprinting (EBB) techniques are therefore the most feasible to employ because they offer a straightforward way to optimize the nozzle diameter and extrusion pressure, allowing researchers to reduce excessive shear stress while still achieving the necessary flow properties and excellent structural bioprinting (Boularaoui et al., 2020). Critically, the EBB technique further mitigates risk associated with harmful processing factors such as organic solvents, laser light, or thermal exposure (Pazhouhnia et al., 2024).

The versatility of EBB allows for the creation of complex, multilayered skin scaffolds by controlling porosity, shape, infill, and cell distribution (Weng et al., 2021). This capability enables the efficient deployment of multiple bioinks for forming the different layers of the skin: one containing fibroblast to form the dermis, followed by another containing keratinocytes to form the epidermis (Díaz et al., 2025). Building upon this principle, Andrade *et al.,* previously demonstrated that 3D bioprinted constructs generated via this EBB approach, consisting of a co-culture model of human keratinocytes and fibroblasts within a high-viscosity bioink, successfully achieved the biomimicry of native skin architecture (Andrade et al., 2025).

This mechanical compatibility makes natural, high-viscosity hydrogels composed of fibrin and alginate highly promising materials for this approach. These materials not only present native adhesion ligands to support cell interaction and mimic desirable ECM properties (such as anti-

inflammatory potential and promoting cell proliferation/differentiation), but also, when combined, their enhanced rheological properties protect cells from excessive shear stress during EBB and rapidly regain rigidity, allowing the scaffold to maintain its structural integrity (Ouyang et al., 2015). This process ultimately facilitates efficient biomimetic tissue morphogenesis and enables essential paracrine signalling (crosstalk) between the fibroblasts and keratinocytes vital for studying cutaneous homeostasis.

1.6 Stratification of a 3D bioprinted scaffold

The adoption of the advanced 3D bioprinted model, as established by Andrade *et al*., provides a crucial platform for studying cutaneous homeostasis. However, for a comprehensive understanding of host-microbe dynamics on a 3D bioprinted model, the formation of the SC within the construct is essential. The SC is the outermost layer of the stratified epidermis, formed when programmed keratinocytes die to create this dead, lipid- and protein-rich layer (Krieken et al., 2016; Matsui et al, 2015). Its presence is critical because it serves as the primary air-liquid barrier where bacteria reside and plays an essential role in priming both the innate and adaptive skin immune systems (Fukuda et al., 2024).

To successfully induce the necessary epidermal stratification and SC formation in a 3D bioprinting construct, the Air-Liquid interface (ALI) methodology is employed. This model utilizes transwell systems with a permeable membrane, positioning one side in contact with liquid culture media while exposing the other to the surrounding air. This approach has been shown to yield more complex and physiologically accurate human skin organoids (Sun et al., 2024), specifically demonstrating that keratinocytes grown under ALI exhibit improved epidermal architecture with cornified cells that closely resemble those seen *in vivo*, thereby greatly enhancing tissue organization (Madison et al., 1988).

Once stratification is achieved, the resultant 3D bioprinted skin models require specific bioprocessing methods for comprehensive analysis. However, because standard 3D histological procedures rely on paraffin embedding, a process that often distorts the delicate hydrogel scaffold structure, optimization of the hydrogel bioprocessing is crucial to successfully perform the necessary staining procedures (Ruan et al., 2013).

1.7 Bioprocessing of a 3D bioprinted skin model

Histology is the established and accepted technique for the microscopic study of tissues and organs, a methodology directly translated to analyse 3D tissue scaffolds. This comprehensive process involves the preparation of thin tissue sections, the application of various stains, and subsequent microscopic examination (Gurina et al., 2025). However, the water-rich and polymeric nature of hydrogels makes them highly sensitive to routine histological procedures, specifically paraffin embedding. This is problematic because the standard method involves dehydration with ethanol, which generally causes the collapse of the hydrogel structure. Furthermore, the hydrophobic characteristic of the paraffin wax often leads to incomplete infiltration, making subsequent sectioning extremely difficult (Ruan et al., 2013).

Cryoslicing is an alternative histological technique that requires freezing the tissue for slicing at approximately -20 ºC (Zhou et al., 2013). This method requires cryopreservation to prevent the formation of ice crystals, which can severely alter cellular and scaffold integrity. To address this, various strategies for tissue preservation can be employed; for instance, Yang *et al.,* demonstrated that using a graded concentration of sucrose solution for cryoprotection significantly improves the integrity of the hydrogel construct and allows for correct embedding with compounds like Optimal Cutting Temperature (O.C.T). This optimized approach ultimately produces complete and high-quality tissue slicing (Ragauskas et al., 2025).

1.7.1 Staining hydrogel construct slices

Once successful slicing has been performed, the obtained 3D slices are subjected to specific staining procedures and subsequent microscopic examination, which are essential for evaluating the model's biological outcome. Hematoxylin & Eosin (H&E) staining serves as the standard histological method, first used to verify keratinocyte maturation and evaluate the formation and proper alignment of the multistratified epithelium (Gangatirkar et al., 2007). To further assess the scaffold's structure, Safranin-O is employed to evaluate the ECM. As a cationic dye, Safranin-O binds specifically to negatively charged components like acidic proteoglycans and glycosaminoglycans (GAGs) within the hydrogel, yielding a distinct reddish-orange stain. This visualization is critical for quantifying the production of these matrix components, which contributes significantly to the overall stability and barrier function of the scaffold, thus relating directly to the expected cross-linked nature of the stratum corneum's (Lee et al., 2016).

Furthermore, 4’,6-diamidino-2-phenylindole (DAPI) fluorescent staining was used to bind A-T rich regions of deoxyribonucleic acid (DNA). This allowed for the identification of viable cell nuclei situated beneath the stratum corneum, a layer composed of acellular, enucleated corneocytes (Hermsmeier et al., 2018). This contrast is essential for confirming terminal differentiation, as absence of DAPI signal in the uppermost layers indicates the successful transition to a cornified barrier.

Finally, for infection models, the Gram staining is fundamental for acknowledging and phenotypically characterizing the bacteria present and confirming their location within the SC (Smith et al., 2005).

1.7.2 Quantifying Functional Host-Microbiome Interactions

While microscopy provides visual confirmation of bacterial presence, it cannot capture the physiological consequences resulting from the interaction between cutaneous cells and the inoculated microbiome at the surface of the construct. Therefore, it is necessary to evaluate the biochemical signaling triggered by the presence of these microorganisms. Cytokines are small, secreted proteins that modulate the behavior of immune cells and other cell types through their ability to interact with a variety of cellular receptors, thereby initiating signaling and protein synthesis (Werner et al., 2003). Consequently, they contribute to the regulation of reepithelialization, tissue remodeling, and the reestablishment of homeostasis (Morán et al., 2013).

Cytokine assays serve as a functional methodology that allows for the detection of protein production before and after bacterial inoculation, providing a framework of essential cellular functions such as growth, differentiation, tissue remodeling, and apoptosis (Whiteside, 2002). This comprehensive screening permits acknowledging if the 3D model functions as a biological network where interactions between the cells and the microbiome occur, effectively demonstrating that the construct serves not only as a structural mimic but also as a functional tissue, capable of restoring the cutaneous barrier and maintaining a stable homeostatic environment through active molecular communication.

1.8 Conclusion and outlook

Even though chronic wounds represent a persistent and costly public health challenge, treatments for them rely on outdated and often limited procedures. This highlights the urgent necessity to develop effective biotherapies that improve patient outcomes. However, many of the models used to develop biotherapies such as 2D and animal models are limited in mimicking the physiological complexity of the skin and are hindered by species-specific differences.

Furthermore, they fail to adequately consider the crucial synergy that exists between the host and the microbiome in establishing a homeostatic or dysbiotic microenvironment, which can dictate whether a chronic wound recovers efficiently and effectively or enters a cycle of vicious inflammation.

The 3D bioprinted skin model addresses this gap by functioning as a biomimetic *in vitro* testing platform for evaluating potential chronic wound therapies in a controllable environment. The primary objective of this work is to develop a 3D bioprinted stratified skin model that is both accessible to produce and easy to replicate, providing a stable architecture for studying the complex microbiome and cutaneous cell interactions *in vitro*.

Achieving this required a comprehensive approach: beyond developing the stratified 3D construct itself, it was necessary to optimize tissue engineering bioprocesses to successfully handle full-thickness, high-viscosity hydrogels. These optimizations ensure that the constructs are robust enough for efficient testing and possess the high degree of reproducibility required for rigorous analysis.

Furthermore, a cytokine screening was performed to demonstrate that the construct moves beyond mere structural mimicry of human skin. While high levels of expression were not observed, the presence of factors critical for regulating homeostasis demonstrated that the 3D bioprinted model serves as a functional biological network, capable of sustaining synergetic crosstalk between the host and microbiome to promote a homeostatic microenvironment and ensure the maintenance of the cutaneous barrier without inflammation.

Ultimately, this comprehensive approach provides a crucial standardization for the creation, application, and analysis of 3D skin models. By democratizing additive manufacturing and establishing a platform where researchers can quantitatively evaluate how the microbiome

"primes" the host response or triggers inflammation, this work fosters more efficient innovation for future tissue engineering applications and the development of disruptive biotherapies.

CHAPTER 2- MATERIALS AND METHODS

2.1 Cell culture of Keratinocytes and Fibroblasts

Primary epidermal keratinocytes (HEKa) extracted from normal human skin from a female, 65-years-old donor (purchased from ATTC, Cat. No. PCS-200- 011, Lot: 70024770, ATCC, Manassas, VA, USA) were cultured in a vented T-75 flasks in 15 mL of Dermal Cell Basal Media (ATCC, Cat No. PCS-200- 030) supplemented with Keratinocyte Growth Kit (ATCC, Cat No. PCS-200- 040). The cultures were maintained at 37°C and 5% of CO_2. The media was changed every two days until the cells reached 70-75% confluency. For subculturing, the cells were rinsed three times with 5.0 mL of Dulbecco's Phosphate-Buffered Saline (DPBS) (R&D Systems, Cat. No. B30250) and incubated with 5.0 mL of Trypsin- Trypsin-ethylenediaminetetraacetic acid (EDTA) (ATCC, Cat. No. PCS-999-003) for two minutes, ensuring to evenly covered the entire cell culture surface with the Trypsin-EDTA solution. Subsequently, 4.0 mL of the solution was then removed, and the flasks were incubated for five minutes at 37°C and 5% of CO_2. The flasks were then gently rocked for two minutes to ensure complete cell detachment. Once detached, the cells were neutralized using an equal volume of neutralizing solution per flask, consisting of 5% Fetal Bovine Serum (FBS) (Millipore Sigma, Cat. No. F1051) in Phosphate-buffered saline (PBS) (ThermoFisher Scientific, Cat. No. J61899.AP). The cell suspension was transferred to a 50 mL conical tube and centrifuged at 150xg for five minutes. Finally, the pellet was resuspended in 1.0 mL of supplemented Dermal Cell Basal Medium and seeded into new flasks at a density of 5000 cells per cm^2 (1.0×10^6 cells), according to the manufacturer's datasheet.

Human dermal fibroblast (HDFs) extracted from normal human facial skin from a Caucasian female 55-years-old donor (purchase from Cell Applications Inc, Cat. No. 106- 05, Lot: 1515) were cultured in a vented T-75 flask in 15 mL of Fibroblasts Growth Medium (ready to use; Cell Applications Inc, Cat. No. 116-500). The cultures were maintained at 37°C and 5% of CO_2. Media was changed every two days until the cells reached 75-80% confluency. For subculturing, the cells were rinsed three times with Hank's Balanced Salt Solution (HBSS) (ThermoFisher Scientific, Cat. No. 14-175-095). To initiate detachment, 5.0 mL of Trypsin-EDTA (Cell Applications Inc., Cat. No. 070-100) was added for two minutes to ensure the solution evenly covered the entire culture surface. Subsequently, 4.0 mL of the trypsin solution was removed, and the flasks were incubated for five minutes at 37°C and 5% of CO_2. The flasks were then gently rocked for two minutes to ensure complete cell detachment. Following detachment, the trypsin activity was neutralized using an equal volume of Trypsin Neutralizing Solution (Cell Applications Inc., Cat. No. 071-100) per flask. The suspension was transferred to a 50 mL conical and centrifuged at 220xg for five minutes. The pellet was resuspended with 1.0 mL of Fibroblasts Growth Medium, and it was inoculated at new flasks 5000 cells per cm^2 (1.0×10^6 cells), according to the datasheet.

2.1.2 Co-culture with customized media

Five days prior to bioprinting, the specific media in the flasks of both Primary epidermal Keratinocytes and Human Dermal Fibroblasts were replaced with a single customized media for both cell types. This media was composed of Dulbecco's Modified Eagle Medium (DMEM) high glucose, GlutaMAX Supplement, and pyruvate (ThermoFisher Scientific, Cat.No. 10569-010), and contained both the keratinocyte supplement (Human Keratinocyte Growth Supplement, HKGS, Cat. No. S0015, ThermoFisher Scientific) and the fibroblast supplement (Low Serum Growth Supplement, LSGS, Cat. No. S00310, ThermoFisher Scientific). The purpose of this shift

was to allow the cells to climatize and ensure they could coexist in the same bioprinted construct, as this customized formulation not only provided the necessary nutrients but also actively promoted the cells to proliferate and sustain viability throughout the *in vitro* maturation phase (Andrade et al., 2025). This simultaneous growth and development of both cell lines ultimately improved the overall stability and function of the resulting construct, enabling subsequent analysis under ALI conditions for fourteen days and microbial co-inoculation studies.

2.2 Bioprinting an Epidermal/ Dermis scaffold

2.2.1 Bioink and Crosslinker preparation

To make the bioink we prepared TissuePrint high-viscosity fibrin-based bioink (TissuePrint-HV Kit—Axolotl Biosciences) based on the protocols Chrenek *et al*., and Perez *et al.* It was formulated with fibrinogen (Sigma Aldrich, Cat. No. 341578-500MG) prepared at a concentration of about 50 mg/mL in Tris-Buffered saline (TBS) solution. The TBS was prepared at pH 7.7 with a final reagent composition of 27.7 mM Tris hydrochloric acid (Tris HCl) (VWR Chemicals, Cat. No. 22J175305), 5.3 mM Tris(hydroxymethyl)aminomethane (Tris base) (ThermoFisher Scientific, Cat. No. 198252), 136.9 mM Sodium chloride (NaCl) (Acrōs Organic, Cat.No A0425202), and 2.7 mM Potassium chloride (KCl) (Caledon, Cat.No.73495). The resulting solution was sterilized using a 0.2 µm syringe filter prior to use. Alginate 5% (Cellink Cat. No. IKA325000503) was added to improve the mechanical properties of the bioink. Genipin (Sigma Aldrich, Cat. No G4796-25MG) was reconstituted at a concentration of 25 mg/mL in di-methyl sulfoxide solution (DMSO) (Sigma Aldrich, Cat. No. D2650-5X5ML). The final concentration in the bioink for fibrinogen, alginate, and genipin was 20, 1.0, and 0.3 mg/mL, respectively (Andrade et al., 2025; Chrenek et al., 2022; Restan Perez et al., 2023). The HEKa and HDF were mixed with

the bioink at a concentration of 2.0×10^6 of each cell type per 1.0 mL of bioink. Furthermore, the crosslinker solution consisted of 20 mg/mL of calcium chloride ($CaCl_2$) (Acrōs Organics, Cat. No.10043-52-4), thrombin at 1.7 U/mL (Sigma Aldrich, Cat. No. T7009-1KU), and chitosan (Sigma Aldrich, Cat. No. 9012-76-4) at 0.075% w/v. Prior to combining all components of the crosslinker, $CaCl_2$ was prepared at a concentration of 20 mg/mL in sterile TBS. Thrombin was reconstituted at a concentration of 1000 U/mL in sterile TBS. Chitosan was added to improve the viscosity of the crosslinker solution and was pre-pared at a concentration of 25 mg/mL using 1.0% glacial acetic acid, and the pH was adjusted to 7.4 using β-glycerophosphate(β- GP) (Sigma Aldrich, Cat. No. G9422-100G) The crosslinking solution was then prepared and sterilized by filtering using 0.2 μm syringe filters. The buffer solution consisted of a TBS solution.

2.2.2 Bioprinting methodology

All bioprinting was performed under sterile conditions using the BIO X extrusion-based printer (Cellink, Cat. No. 16110020717). The printer was outfitted with two pneumatic printheads (cartridges with end and tip caps with 3.0 mL—Cat. No. CSC010300102, Cellink) and 22 G (0.41 mm) sterile standard conical bioprinting nozzles (Cellink, Cat. No. NZ4220005001). The constructs were printed using a custom 3D model, as shown in figure 4. The constructs were 7.07 X 7.07 X 5.9 mm in size, and were printed with 65% rectilinear infill, 15 mm/s speed, and 11kPa of pressure.

The two printheads were loaded separately: the first with HDF cells in bioink and the second with HEKa cells in bioink, both at a concentration of 2.0×10^6 cell/mL. This setup resulted in a bioprinted co-culture construct mimicking the physiological proportions of the dermis and epidermis, consisting of fourteen stacked layers. The layering strategy began with four layers printed using the first printhead (Dermis layer). Subsequently, the second printhead was

automatically engaged to alternate and print ten layers on top, with the final four of these layers forming a solid concave surface (Epidermis layer). This layered design served the dual purpose of replicating the natural composition of human skin while promoting SC formation by the skin cells and facilitating future interaction with the microbiome during subsequent co-inoculation.

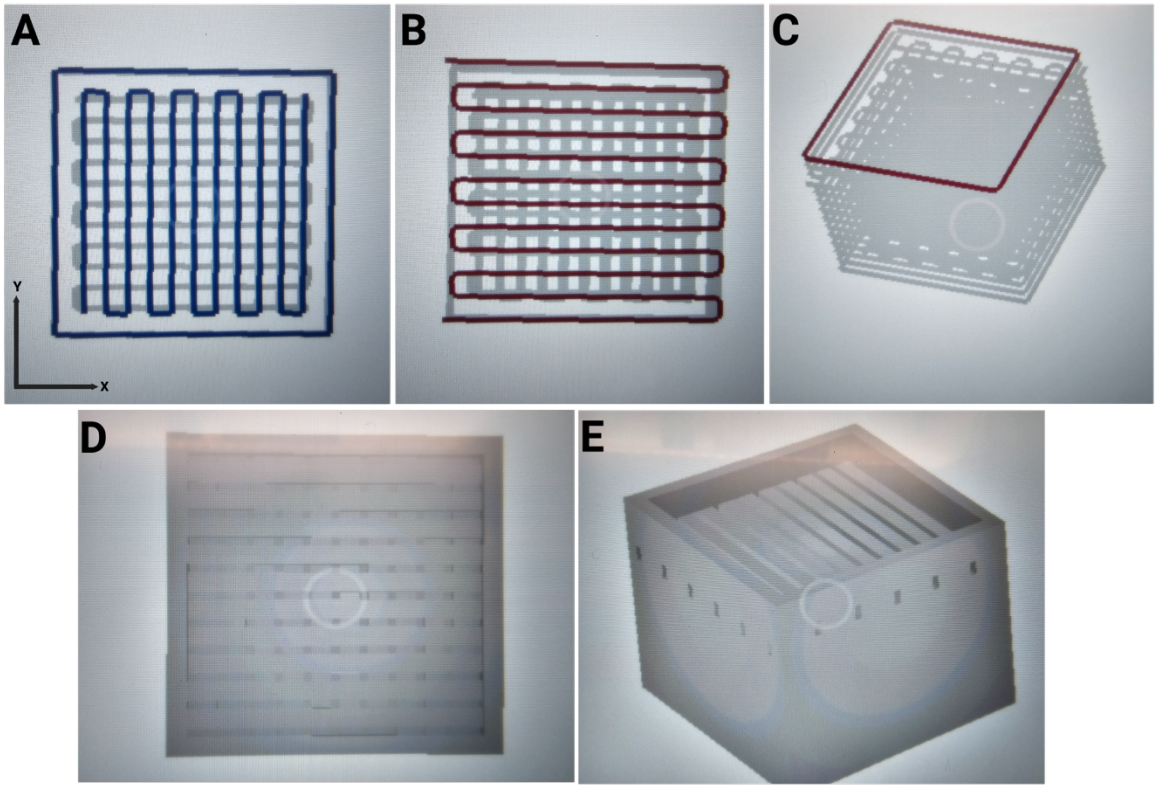

Figure 4. 3D modeling and bioprinting parameters for stratified skin constructs. Constructs were fabricated via a BIO X extrusion based bioprinter using a dual-nozzle setup (22 G) at 11 kPa and 15 mm/s. The 14-layer architecture consists of a 4-layer dermal base (HDF) and 10 epidermal layers (HEKa) at 2.0×10^6 cell/mL. The design utilizes a 65% rectilinear infill, transitioning to a custom dense infill surface in the final four layers to promote stratum corneum (SC) formation and facilitate microbial interaction. **(A) Top view of the rectilinear infill for the top layers, illustrating the specific toolpath. (B) Top view of the rectilinear infill for the middle layers, showing the alternating internal pattern. (C) Isometric view of the sliced construct, demonstrating the stacked internal architecture. (D) Top view of the final 3D model, representing the surface geometry. (E) Isometric view of the completed 3D model**, showing the full physiological proportions. Created in BioRender. Tuffs, S. (2026) https://BioRender.com/undefined

The constructs were printed in a 6-well plate (CellStar, Cat. No. 657160) directly onto 2.0 mL of 0.5% agarose (FroggaBio, Cat. No. A87-500G) support bath to stabilize the bioink during extrusion and precise scaffold formation. Following printing, the crosslinker solution, held in 10 mL syringe fitted with a 22 G needle, was slowly injected in a circular motion around the constructs, with approximately 2.0 mL of crosslinker employed/poured, taking care not to touch the construct with the needle. The crosslinker was allowed to sit for 20-30 minutes. Once the constructs appeared visibly opaque or whitish, they were transferred to a 6-well plate containing TBS to wash and remove the excess agarose surrounding the construct. Subsequently, the constructs were transferred to a 12-well plate (CellStar, Cat. No.665180) containing 2.0 mL of customized media and incubated at 37°C with 5% CO_2 for two days before moved into a 12-well transwell plate for further fourteen days maturation (Díaz et al., 2025).

2.2.3 Air liquid interface (ALI) stratification formation

On the second day post-embedding, the constructs were transferred into a 12-well transwell plate (Sigma Aldrich, Cat. No. CLS3460-48EA) to initiate culture under ALI methodology. This setup was achieved by positioning the bottom part of the construct (the HDFs layers) in direct contact with the transwell membrane, leaving the top layers (the HEKa layers) exposed to the ambient oxygen. The constructs were cultured using this methodology for fourteen days, with the 500 µL of customized media being refreshed every second day. Following this maturation period, the constructs were divided into four different experimental groups for microbial monoculture inoculation and co-inoculation: a Control group without bacteria, monoculture with *S. aureus*, monoculture with *S. epidermidis*, and a co-inoculation group with both *S. aureus* and *S. epidermidis*.

2.3 Inoculation of bacteria into the construct

2.3.1 Bacterial culture preparation

Two days before inoculation of bacteria into the construct, the single strains of *S. aureus* (9MW2 +GFP., BEI Resources, Cat. No: NR-46054) and *S. epidermidis* (RP62a., BEI Resources, Cat.No: NR-45879) were cultured (Christensen et al., 1982; Fey et al., 2003). Preparation began by picking a single bacterial colony from a tryptic soy agar (TSA) (Sigma Aldrich, Cat. No.22091-500G) plate and let it growth overnight (16-18 hrs) in 5.0 mL of sterile tryptic soy broth (TSB) (Sigma Aldrich, Cat. No. 22092-550G) with shaking at 200 rpm. Following this, 1.0 mL of the overnight culture was transferred into 50 mL of fresh sterile TSB and incubated for four hours at 37°C with shaking. Subsequently, 10 mL of this culture was transferred into a 15 mL conical tube and centrifuged at 4000xg for 10 minutes. The resulting pellet was resuspended with 10 mL of PBS and centrifuged again. The final bacterial pellet was then resuspended again in 10 mL of PBS, after which the optical density at 600 nm (OD_{600nm}) of the culture was adjusted to 0.1 using spectrophotometer.

2.3.2 Inoculation of the constructs

The bacterial cultures were standardized such that an $OD_{600\ nm}$ of 0.1 corresponded to a concentration of 5×10^8 CFU/mL. For infecting the constructs, a total dose of 5×10^6 CFU was added per construct. For the co-infection group, this dose comprised 2.5×10^7 CFU of *S. aureus* and 2.5×10^7 CFU of *S. epidermidis.* Based on the standard 150 µL volume of the bioprinted construct, this final inoculation density translates to approximately 3.33 x 10^8 CFU/cm^3.

Inoculation was performed by pipetting 2.5 µL of the respective bacterial suspension (*S. aureus* only, *S. epidermidis* only, or co-infection) at the surface of the construct. Furthermore, the

inoculated constructs were then incubated at 37°C with 5% CO_2 for forty-eight hours. Once, the inoculation period was completed, the constructs were fixed with 4% Paraformaldehyde (PFA) (ThermoFisher Scientific, Cat. No. J61899AP).

2.4 Cytokine Assay

After fourteen days of the constructs being in ALI culture, approximately 500 µL of the customized cultured media was collected from each group (Control group without bacteria, monoculture with *S. aureus*, monoculture with *S. epidermidis*, and a co-inoculation group with both *S. aureus* and *S. epidermidis*) using 1.0 mL Eppendorf tubes and stored at -20°C. Forty-eight hours post-bacterial inoculation, a second collection of approximately 500 µL of the customized media was performed for all groups and stored at -20°C. This resulted in two distinct set of conditioned media: pre-inoculation and post-inoculation.

All the collected media sets were sterilized using 0.2 µm filters. Subsequently, 75µL of the sterilized media was diluted with 75µL of PBS in 1mL Eppendorf tubes. The final experimental design comprised eight distinct groups, each with four biological replicates (A, B, C, and D), categorized as: A1 (Control pre-inoculation), A2 (Control post-inoculation), A3 (*S. aureus* monoculture pre-inoculation), A4 (*S. aureus* monoculture post-inoculation), A5 (*S. epidermidis* monoculture pre-inoculation), A6 (*S. epidermidis* monoculture post-inoculation), A7 (Co-inoculation pre-inoculation), and A8 (Co-inoculation post-inoculation).

The samples were sent to Eve Technologies for further analysis using the Human Cytokine/Chemokine Panel A 48-Plex Discovery Assay® Array (HD48A). This multiplex assay allows for the simultaneous detection of 48 biomarkers from a small sample volume, including essential targets such as IFNγ, TNF- α, Transforming Growth Factor alpha (TGF- α), Vascular Endothelial Growth Factor A (VEGF-A), IL-1β and Interleukin-10 (IL-10), providing

comprehensive coverage of the immune and inflammatory response (Eve Technologies, 2025). The analysis provided dual data points for each analyte: Fluorescence Intensity (FI), representing the median reporter signal, and Observed Concentration, calculated via a validated standard curve. Only analytes with concentrations falling within the assay's sensitivity range (0.14 – 50.78 pg/mL) were included in the final dataset.

To quantify functional signaling shifts between the control, *S. epidermidis* monoculture*, S. aureus* monoculture, and co-inoculated groups, multiple paired t-tests were performed in GraphPad Prism. This design was selected because the analysis compared the means of two matched observations, specifically, the pre- and post-inoculation states of each individual construct.

This parametric approach assumes that the distribution of the before-after differences follows a Gaussian distribution. By focusing on the differences within each construct, the test effectively controls for inherent experimental variability across the biological replicates. Following the "Planned Comparisons" framework, the significance threshold was set at $\alpha=0.05$ for each individual comparison (*Prism_v5_Statistics_Guide*, 2007.)

2.5 Cryoslicing the constructs to perform staining assays

2.5.1 Cryopreservation of the hydrogels

Once fixed, the constructs were transferred into a 12-well plate to begin cryopreservation infiltration, following an optimized protocol derived from Yang *et al*., for high-viscosity fibrin hydrogels (Ragauskas et al., 2025). The process started by embebbeding the constructs in 1.0 mL of 5% w/v of sucrose (Anachemia, Cat. No.87688-380) in PBS for one hour at 21°C. The sucrose concentration was then gradually increased by adding 30% w/v of sucrose in PBS every thirty

minutes, adjusting the 5% and 30% sucrose ratios in ascending concentrations of 2:1, 1:1 and 1:2, before storing them at 4°C for three days. Following cryoprotection, the sucrose was carefully removed, and infiltration with O.C.T (ThermoFisher Scientific, Cat. No. 23730571) was initiated in a stepwise manner: first by adding 1.0 mL of 30% sucrose and 0.5 mL of O.C.T for one hour; and finally, adding 1.0 mL of pure O.C.T and storing the constructs at 4°C overnight. The cryopreservation infiltration was completed by removing the previous solution and adding 2.0 mL of purse O.C.T for three hours at 21°C. Refer to the table 1.

Table 1. Adapted Infiltration method for cryosectioning 3D bioprinted constructs.

Step	Solution	Volume	Time
1	5% Sucrose	1.0 mL	1 hour
2	30% Sucrose	0.5 mL	30 minutes
3	30% Sucrose	0.5 mL	30 minutes
4	30% Sucrose	1.0 mL	30 minutes
5	Store infiltrated constructs at 4°C with sucrose solution		3 overnights
6	30% Sucrose-O.C. T	1.0 mL-0.5 mL	1 hour
7	O.C. T	0.5 mL	1 hour
8	O.C. T	1.0 mL	1 hour
9	Store infiltrated constructs at 4°C with sucrose / O.C.T solutions		Overnight
10	O.C. T	2.0 mL	3 hours

2.5.2 Freezing the O.C.T infiltrated constructs

During the final three hours of the infiltration step, a thin base layer of O.C.T compound was added to a Peel-A-Way mold (Polysciences, Cat. No.18646A-1) and frozen at -20°C for one hour. Once the infiltration was complete and the base layer had solidified, a fresh drop of O.C.T was placed onto the center of the mold. The infiltrated constructs were then carefully transferred into the mold using a spatula. As illustrated in Figure 5, the constructs were oriented such that the epidermal layer faced upward, and the dermis was positioned at the base of the mold. Finally, additional O.C.T was added to submerge the constructs completely, and the molds were allowed to freeze thoroughly at -20°C for one hour.

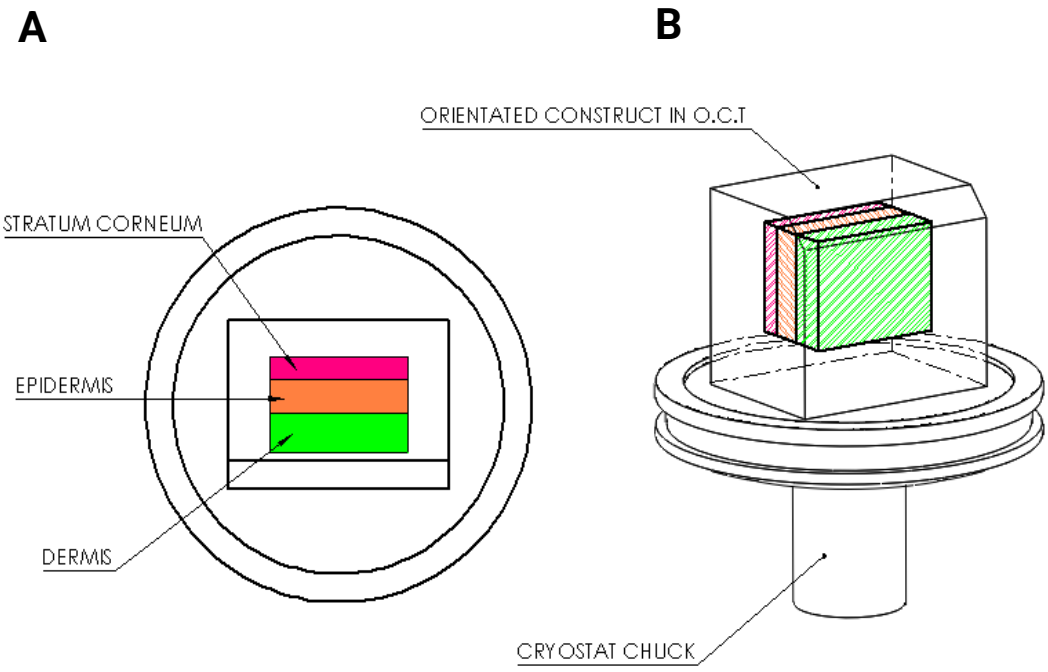

Figure 5. Orientation and cryosectioning of the 3D skin construct. The 3D construct is embedded within a block of O.C.T. compound and mounted onto the cryostat chuck, maintaining its physiological vertical axis. **(A)** Schematic of the stratified layers: Stratum corneum (top), Epidermis (middle), and Dermis (base). **(B)** Mounting orientation for coronal sectioning, where the sample is aligned to allow sequential slicing from the anterior (epidermal/SC) surface toward the posterior (dermal) layer. This specific orientation is critical for preserving the structural relationship between the enucleated barrier and the underlying cellular layers during histological processing.

2.5.3. Mounting and cryosectioning

Before the cryoslicing process started, the cryostat (Leica Biosystem, Cat. No.047140225) was turned on and set to maintain a temperature of -25°C. The cryostat was prepared by inserting a pre-cooled blade into the knife holder and clamping it securely. Next, the embedded mold was attached to the specimen holder. The appropriate clearance angle on the knife holder was adjusted, and the blade was aligned parallel to the glass slide surface. Slices were performed at a thickness of 60µm, with the cryosectioned sections being disposed onto a glass slide (ThermoFisher Scientific, Cat. No.125496C). The glass slide containing the cryosectioned specimen/3D bioprinted construct was then allowed to air dry at 21°C for 15-20 minutes before further processing.

2.6 Staining High-viscosity hydrogels slices

2.6.1 Hematoxylin and Eosin assay

To evaluate the structural integrity of both the honeycomb pattern with 30% infill and the rectilinear pattern with 65% infill density constructs, H&E staining was performed following an optimized protocol adapted from Purkeson *et al.*, specifically for high-viscosity fibrin hydrogels (Purkerson et al., 2023). Starting by rehydrating the cryosections on the glass slides through a three-minute graded ethanol series, starting with two submersions in 100%, then 95%, and finishing with 70%. Following rehydration, the slide was washed with PBS for three minutes. Subsequently, Hematoxylin (Abcam, Cat No. ab245880) was applied for one minute. The slices were then washed with distilled water until the purple colour was no longer coming out, followed by a final rinse in water for five minutes. Subsequently, bluing solution (Abcam, Cat No. ab245880) was added for thirty seconds and washed off with distilled water. The final steps

involved dehydrating the slices by applying 95% ethanol for three minutes, followed by the application of Eosin/Phloxine (Abcam, Cat No. ab245880) for two minutes. Concluding with two separate washes of 95% ethanol and finishing with two washes of 100% ethanol, all for three minutes each. The slides were finally allowed to air dry at 21°C for 15-20 minutes before further analysis using the Brightfield microscope (Zeiss. GBM No.10387) at 20X and 40X magnification and digitized using Microvisioneer ManualWSI 2019B-3S.

2.6.2 DAPI fluorescence staining

The DAPI fluorescence staining procedure began by washing the cryosectioned slices with PBS to remove any residual O.C.T compound. Control slides, which included acellular constructs (without cells) to determine the hydrogel's background fluorescence and constructs without bacteria, were fixed with 95% ethanol for one minute. Following fixation, the slices were stained with 1 mL of DAPI (ThermoFisher Scientific, Cat. No. D1306) solution at a 1:100,000 dilution in PBS for five minutes. The sections were then thoroughly rinsed with distilled water and allowed to air-dry at 21°C for 15–20 minutes in the dark, as DAPI is a light-sensitive reagent. For high-resolution analysis, the sections were imaged using a Cytation 10 microscope (Agilent, Model. No. C10MIPHC2-SN) at 4X and 20X magnification. Fluorescence analysis of the SC and the overall construct was conducted using ImageJ, merging the brightfield and blue channels to visualize the cellular distribution.

2.6.3 Safranin-O assay

The Safranin-O staining was performed using an optimized protocol derived from Guo *et al*., for high-viscosity fibrin hydrogels (Guo et al., 2024). The procedure began by washing the cryosectioned slices with PBS to remove any residual O.C.T compound. The slides were then fixed

with 95% ethanol for one minute. Following fixation, the slices were flooded with Safranin-O solution (Sigma Aldrich, Cat. No.HT90T-1KT) for five minutes. The slices were then thoroughly rinsed with distilled water until the red colour was no longer coming out. The slides were finally allowed to air dry at 21°C for 15-20 minutes. For further analysis, the section was imaged using Brightfield microscope at 20X magnification and digitized using Microvisioneer ManualWSI 2019B-3S.

These digital records served as the basis for morphometric quantification, where the stratum corneum and construct area were manually annotated and measured using the brush tool in QuPath 5.0 (Bankhead et al., 2017). To account for varying slice sizes, the data was normalized by dividing the SC area by the total area of the slice. To ensure the robustness of the resulting measurements, statistical analyses were conducted using GraphPad Prism. Prior to comparative testing, data normality was assessed; the dataset passed the Shapiro-Wilk normality test, confirming a Gaussian distribution. Consequently, the data were treated as parametric, and a One-way ANOVA was used to compare the *S. epidermidis* monoculture, *S. aureus* monoculture and Co-infected groups against the non-inoculated control.

2.6.4 Gram staining assay

The Gram staining was performed using an optimized protocol derived from Xuan Guo *et al*., for high-viscosity fibrin hydrogels (Guo et al., 2024). The procedure began by washing the cryosectioned slices with PBS to remove any residual O.C.T compound. The slides were then fixed with 95% ethanol for one minute. Following fixation, the slices were flooded with Crystal Violet solution (Sigma Aldrich, Cat. No.HT90T-1KT) for one minute. The slices were then thoroughly rinsed with distilled water until the purple colour was no longer coming out. Continuing the process, the slices were flooded with Gram's Iodine Solution (Sigma Aldrich, Cat. No.HT90T-

1KT) for one minute and rinsed thoroughly with distilled water. The critical decolorization step involved adding 95% ethanol for up to ten seconds, or until the purple colour stopped running out. Subsequently, Safranin-O solution was added for five minutes and rinsed thoroughly until the red colour was no longer coming out. The slides were finally allowed to air dry at 21°C for 15-20 minutes, before further analysis using the Brightfield microscope at 20X and 40X magnification and digitized using Microvisioneer ManualWSI 2019B-3S. Methods are summarized in Figure 6.

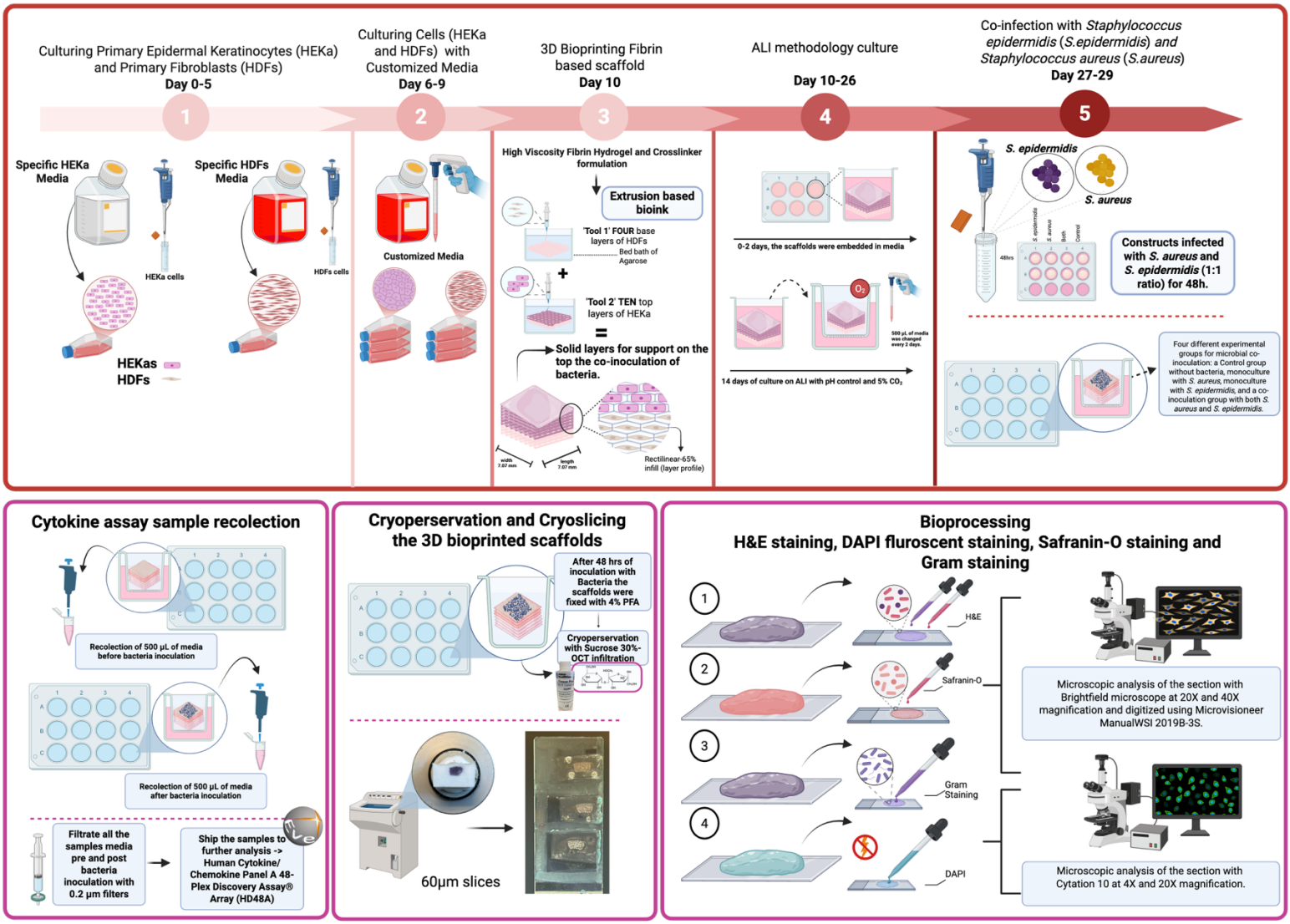

Figure 6. Methodological overview. The process began with the seeding and expansion of primary human epidermal keratinocytes (HEKa) and primary fibroblasts (HDFs) in specialized and customized media. Following expansion, an extrusion-based 3D bioprinting technique was employed to generate a fibrin-based scaffold by layering HDFs at the base and HEKa on the surface to establish the initial tissue architecture. These constructs were matured in an Air-Liquid Interface (ALI) culture for 14 days to promote comprehensive epidermal differentiation and cornification. To evaluate microbial dynamics, the matured constructs were subjected to a 48-hour inoculation period featuring *Staphylococcus epidermidis* (*S. epidermidis*) and *Staphylococcus aureus* (*S. aureus*) in both monoculture and co-infection models. Pre and Post-inculation, media samples were recollected for cytokine profiling to assess the inflammatory response. The constructs then underwent cryopreservation and cryoslicing into 60µm sections for histological characterization. Finally, bioprocessing involved Hematoxylin and Eosin (H&E) staining for structural morphology, DAPI fluorescent staining for nuclear visualization, Safranin-O staining, and Gram staining to identify bacterial localization. Microscopic analysis was performed using brightfield and fluorescence microscopy at 4X, 10X, 20X to 40X magnification to assess tissue integrity and microbial colonization. Created in BioRender. Tuffs, S. (2026) https://BioRender.com/undefined

CHAPTER 3- RESULTS

3.1 Cryopreservation of the high-viscosity hydrogels improve the cryoslicing of the constructs at the Cryostat.

The inherent nature of hydrogel as water-rich, polymeric structures presents a significant limitation for conducting routine histological procedures. Such high hydration makes the construct extremely sensitive, making it difficult to achieve correct sectioning; therefore, it is challenging to proceed with the staining and microscopic examinations required to investigate tissue structure, specific components, or conditions.

To overcome these challenges, a specialized cryopreservation protocol was optimized based on a gradual sucrose to O.C.T infiltration. By transitioning the constructs through ascending ratios of 5% and 30% sucrose (2:2, 1:1 and 1:2), followed by a stepwise integration of O.C.T, internal water was effectively displaced. This methodical approach significantly minimized ice crystal formation, which is the primary cause of structural damage and “shredding” during the freezing process (Ragauskas et al., 2025).

As a result, the cellular and scaffold integrity was preserved, as shown in Figure 7. This optimization was a critical success, as it provided the capability to visualize the scaffold architecture and proceed with the refinement of bioprinting features necessary to achieve correct stratification, ensuring the 3D bioprinted skin model accurately resembles human skin physiology. This was followed by the ability to enable high-resolution visualization of the stratum corneum and the precise mapping of the microbiota at the scaffold surface.

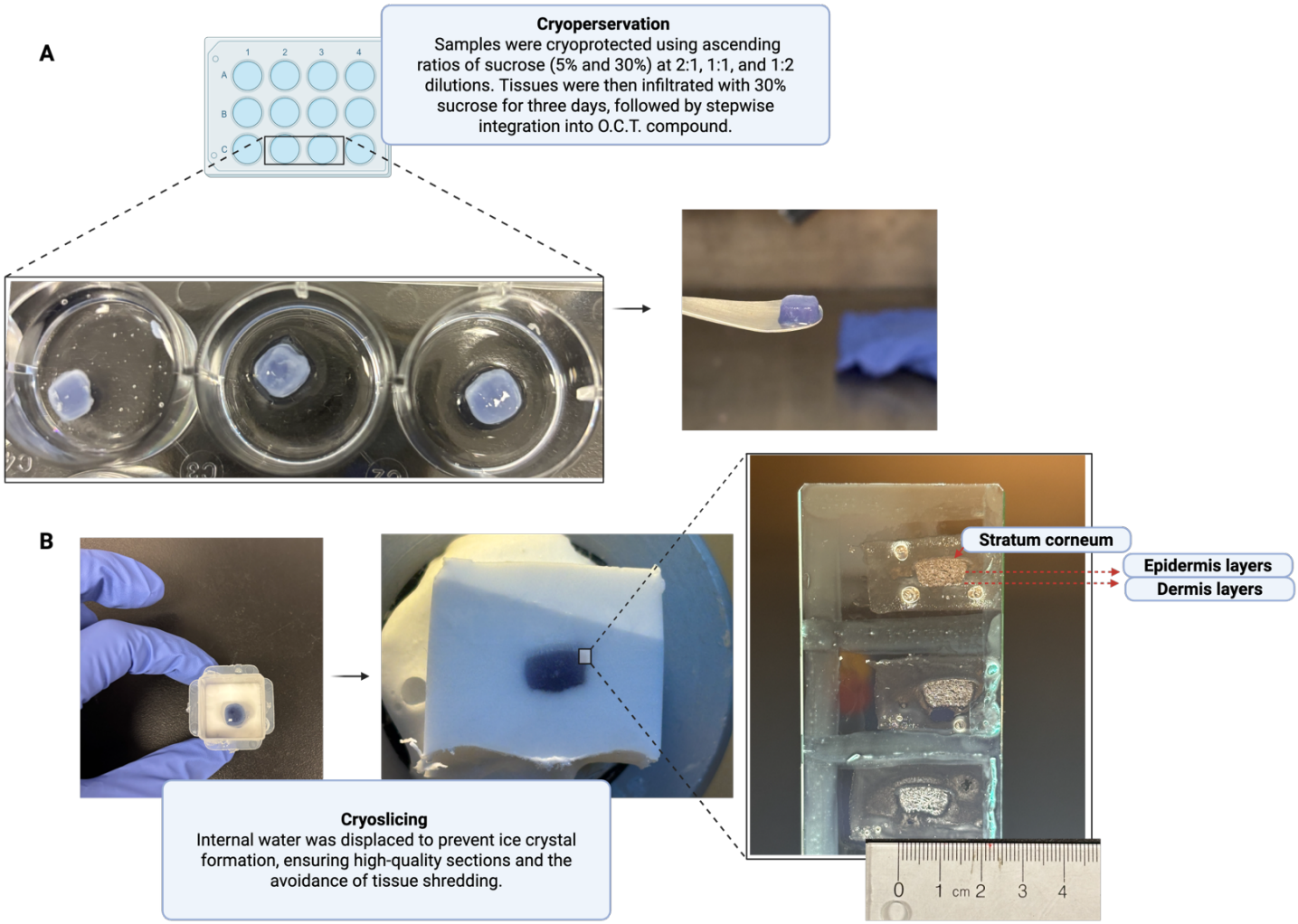

Figure 7. Cryopreservation and cryoslicing optimization of 3D bioprinted skin constructs. **(A)** Methodological workflow designed to overcome the structural fragility of water-rich fibrin hydrogels through a specialized infiltration protocol. **Constructs were transitioned through ascending ratios of 5% and 30% sucrose (2:1, 1:1, and 1:2) followed by stepwise O.C.T. compound integration to effectively displace internal water**. This approach minimized ice crystal formation, preventing the "shredding" typically associated with standard freezing methods. **(B)** Macroscopic and microscopic evaluation of the processed constructs. **The optimized protocol yielded high-resolution 60 µm cross-sections that maintained total structural and cellular integrity.** These sections clearly visualize the preserved, stratified architecture of the model, including the distinct dermis, epidermis layers, and the formation of a defined stratum corneum at the scaffold surface. *Scale bar:* 1.2 cm. Created in BioRender. Tuffs, S. (2026) https://BioRender.com/undefined

3.1.1 Infill adjustment and ALI culture improved the preservation and stratification of the 3D scaffold.

Stratification is an essential component of skin physiology and host response; therefore, a major aim for the 3D construct was to develop an epidermal barrier that closely resembles native skin. This required achieving differentiated layers and an epidermal lipid composition capable of supporting the stratum corneum, where the host microbiome co-habits.

H&E staining was employed to investigate the stratification and correct alignment of these layers within the scaffold. Despite the characteristic non-specific purple staining of the hydrogel matrix, it was possible to evaluate the impact of honeycomb patterns and 30% infill bioprinting features, as well as the embedding culture, on the construct's structural organization. As shown in Figure 8, the initial scaffold architecture failed to support stratification, rendering the structure fragile and unable to form the necessary alignment to support the air interface. For this reason, an improvement in bioprinting features was pursued, transitioning to a rectilinear pattern and 65% infill. Additionally, an ALI culture was introduced two days post-bioprinting, allowing the surface of the construct to remain in contact with oxygen. According to Chettouh-Hammas *et al.*, increasing oxygen levels from physioxia toward hyperbaric conditions significantly increases stratum corneum thickness by facilitating a shift from glycolysis to mitochondrial metabolism. This metabolic transition is crucial for the terminal differentiation of epidermal keratinocytes, resulting in a durable stratum corneum required to build a protective barrier (Chettouh-Hammas et al., 2024).

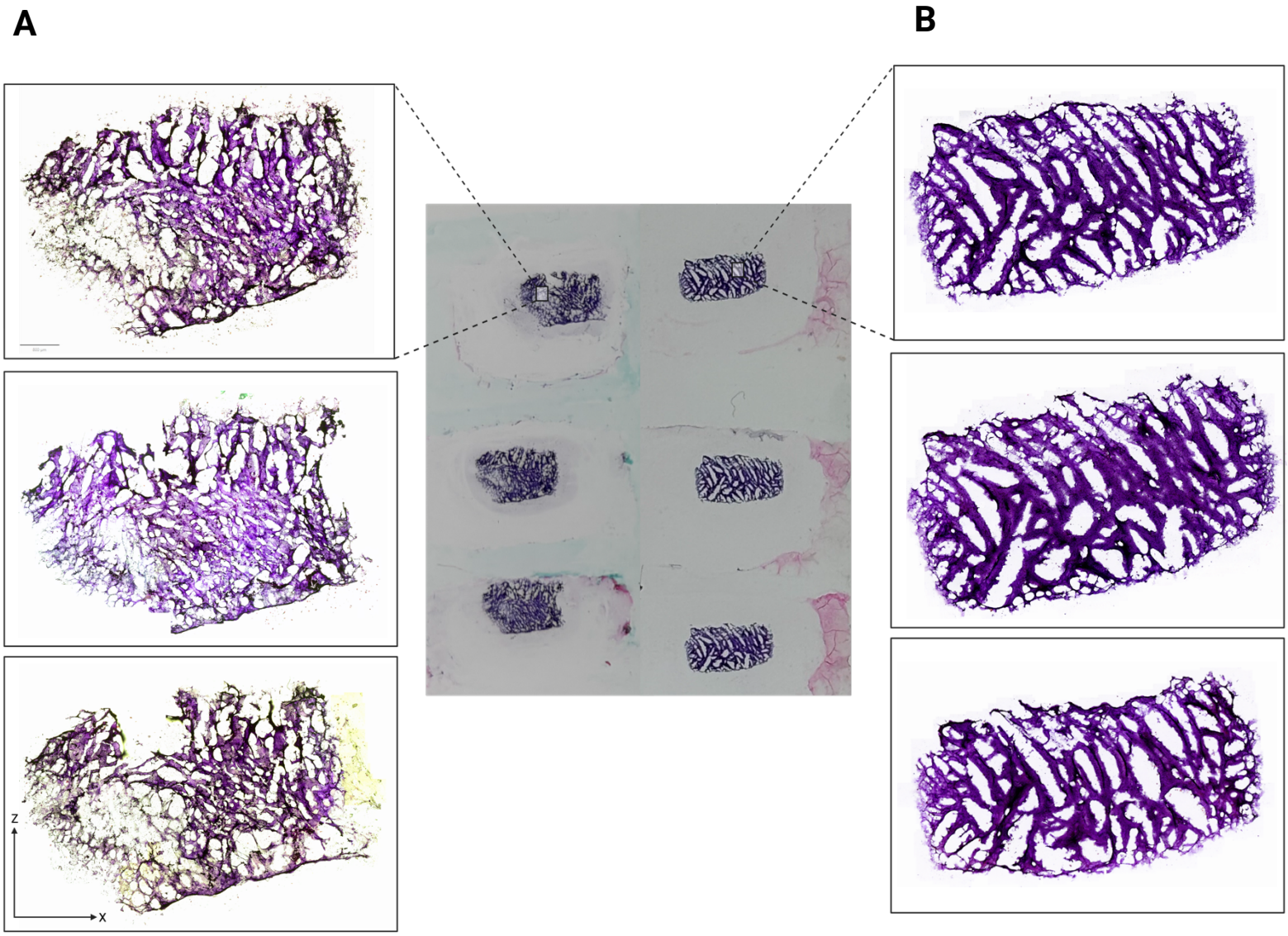

Figure 8. Histological comparison of 3D bioprinted scaffold architectures using H&E staining. (A) Honeycomb pattern with 30% infill density and embebbed culture methodology. H&E staining revealed that the initial scaffold architecture lacked the structural alignment necessary to support the air interface, resulting in a fragile construct that failed to achieve stratification. **(B) Rectilinear pattern with 65% infill density and Air-Liquid Interface culture methodology**.The transition to an increased **infill density and an optimized printing pattern provided the structural integrity required for successful alignment**. *Scale bar:* 800 µm

After fourteen days in ALI culture, H&E staining complemented by DAPI visualization provided clear evidence of structural alignment and the formation of the SC (Figure 9). The DAPI results confirmed this stratification by showing an absence of fluorescence in the upper part of the construct, consistent with the enucleated nature of the stratum corneum, while distinct fluorescence was visualized in the lower layers. Together, these imaging techniques allowed for the refinement of printing parameters necessary to achieve accurate stratification, ensuring the model successfully resembles human skin physiology.

A

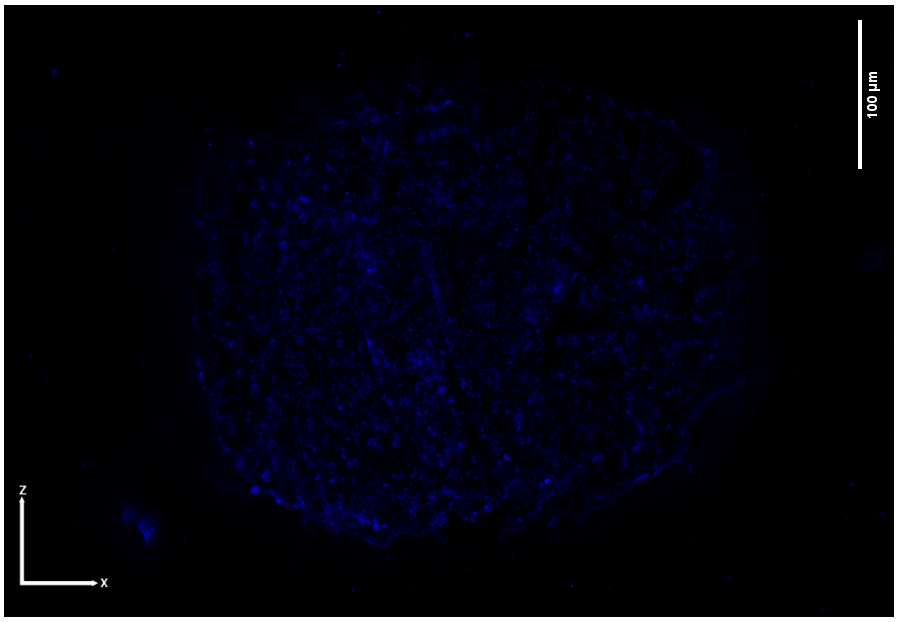

DAPI

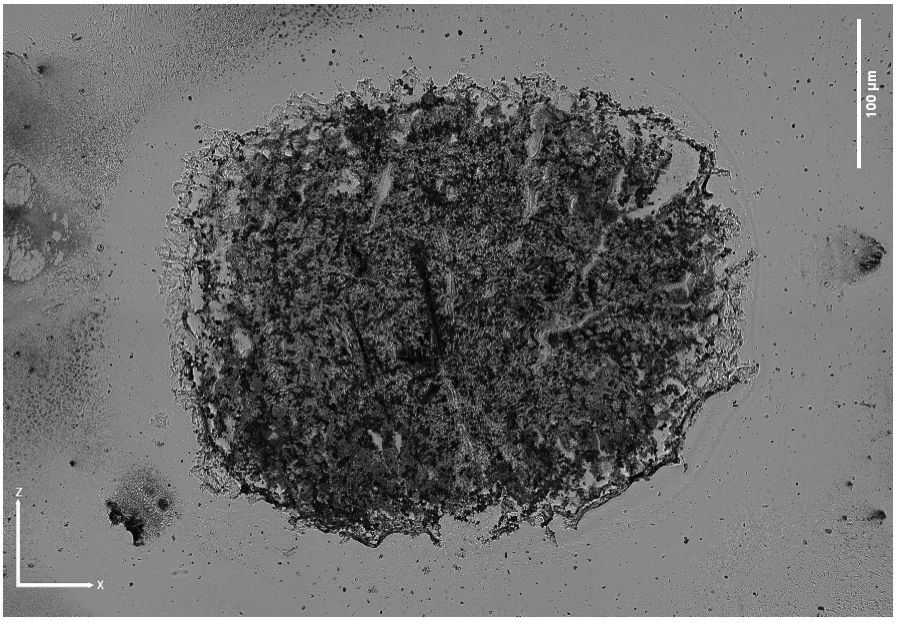

Brightfield

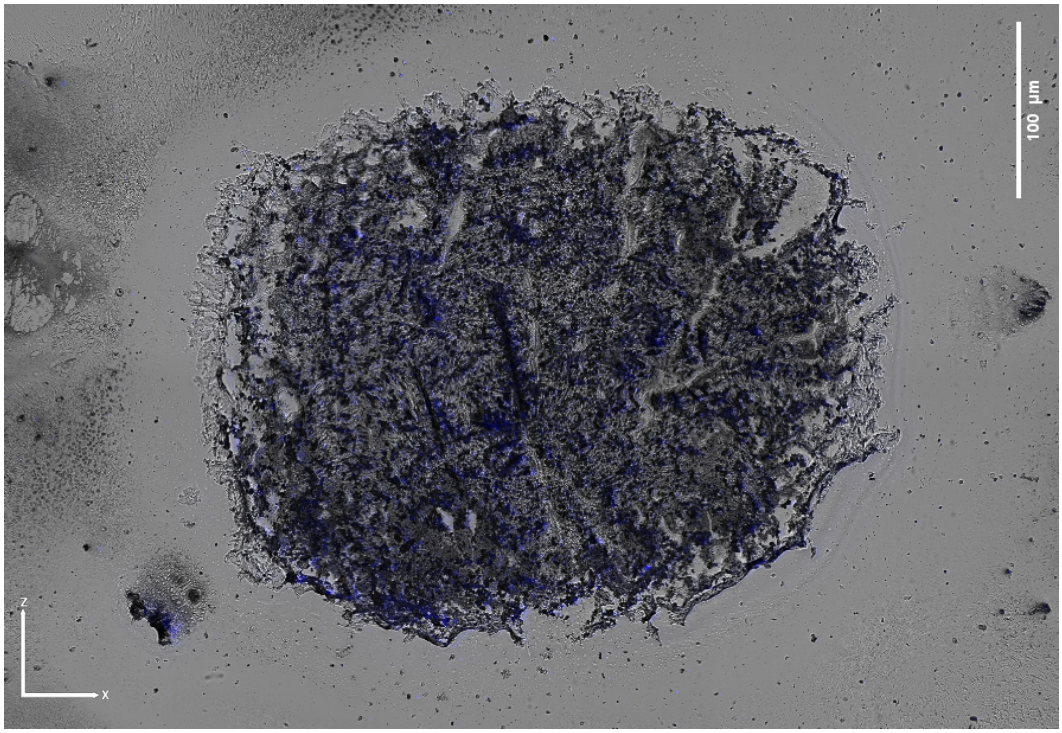

Dermal Structure

Merge

B

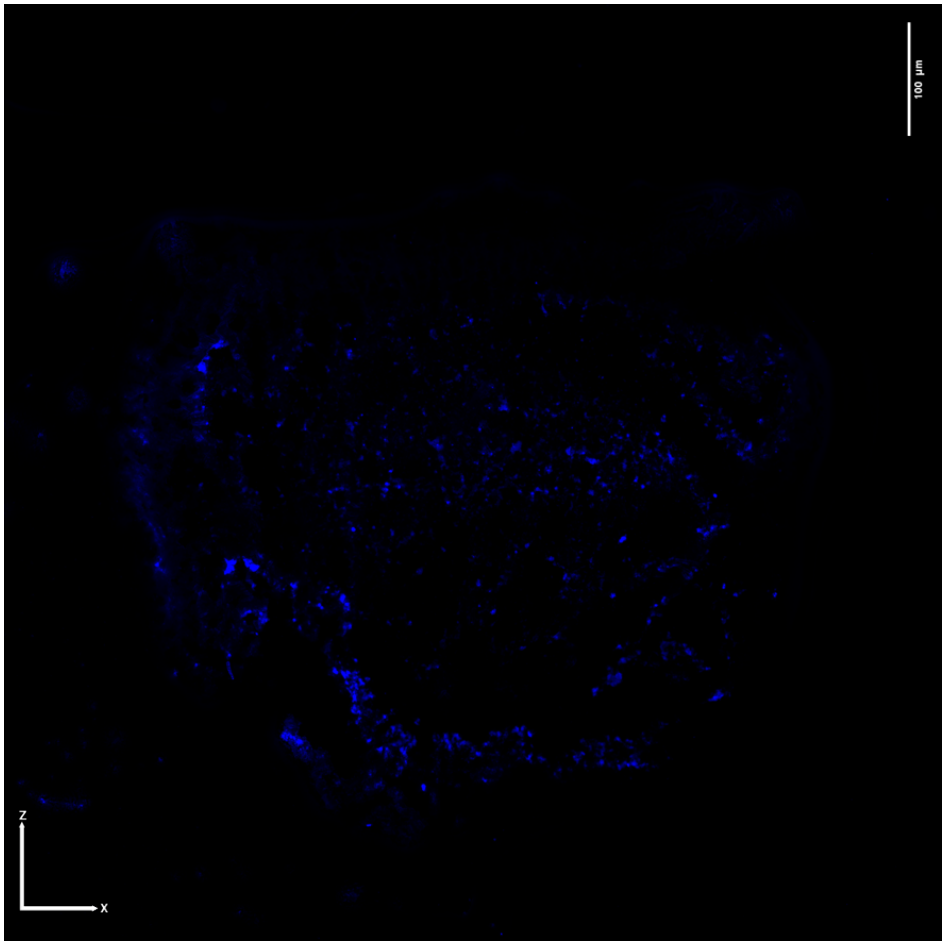

DAPI

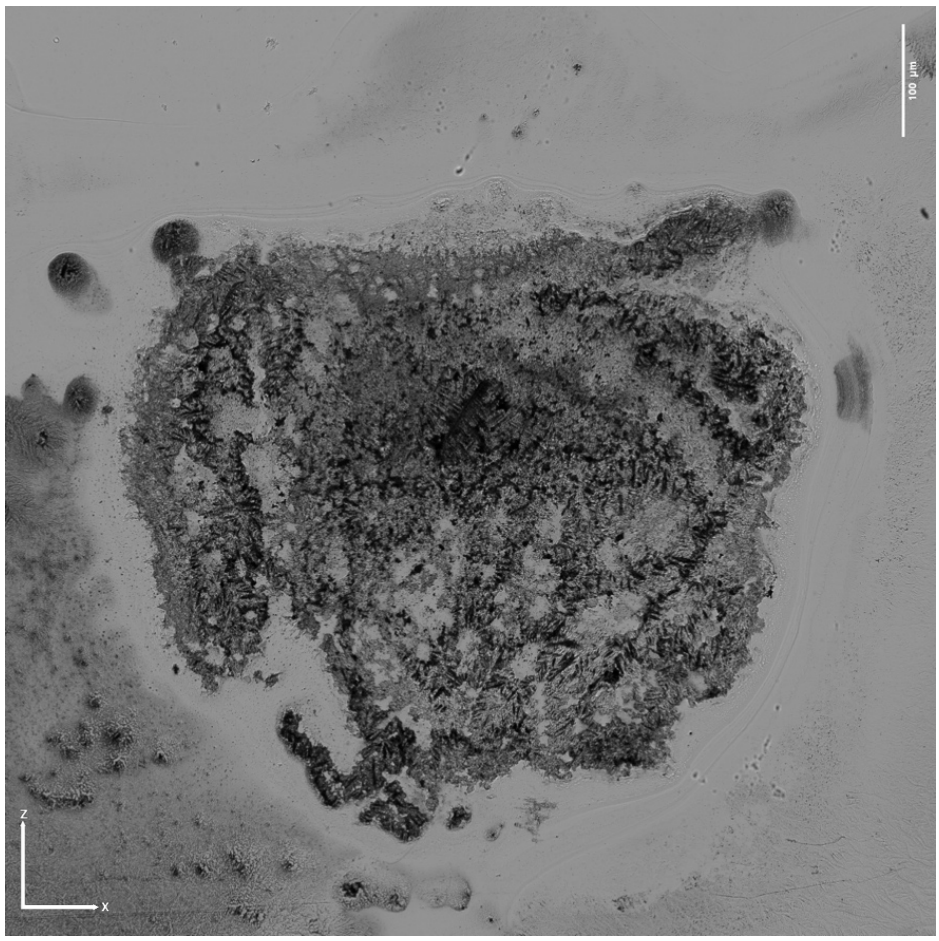

Brightfield

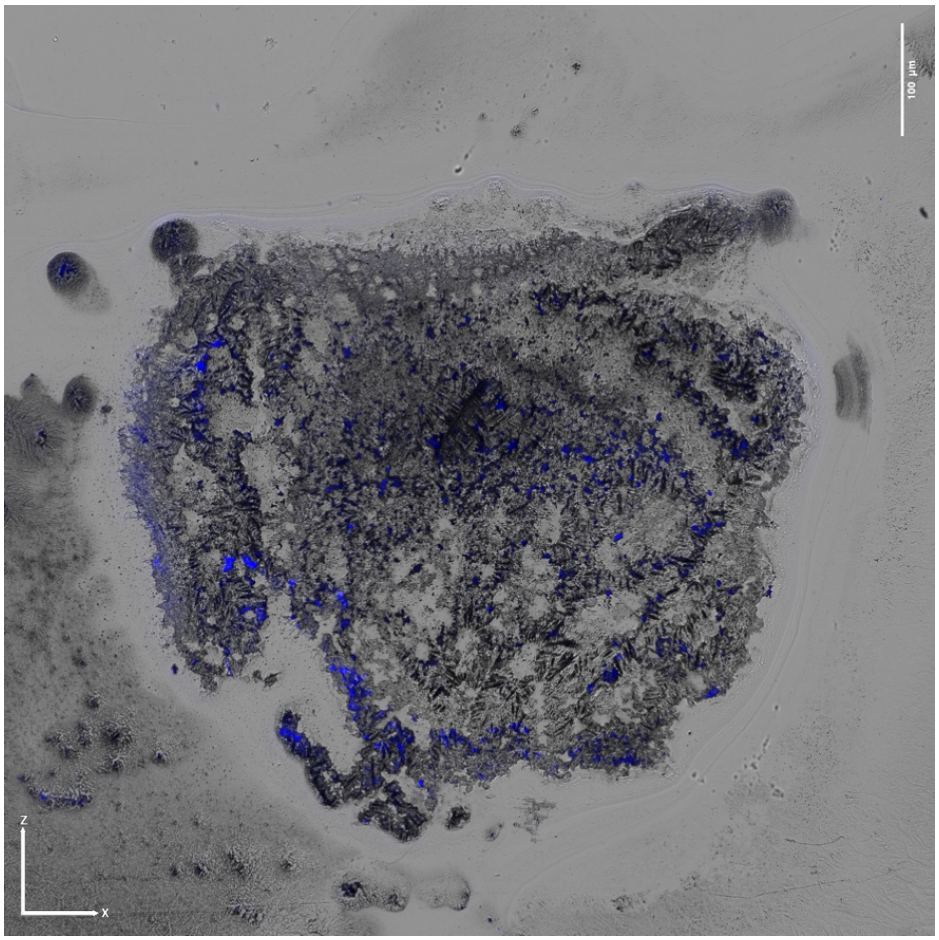

Merge

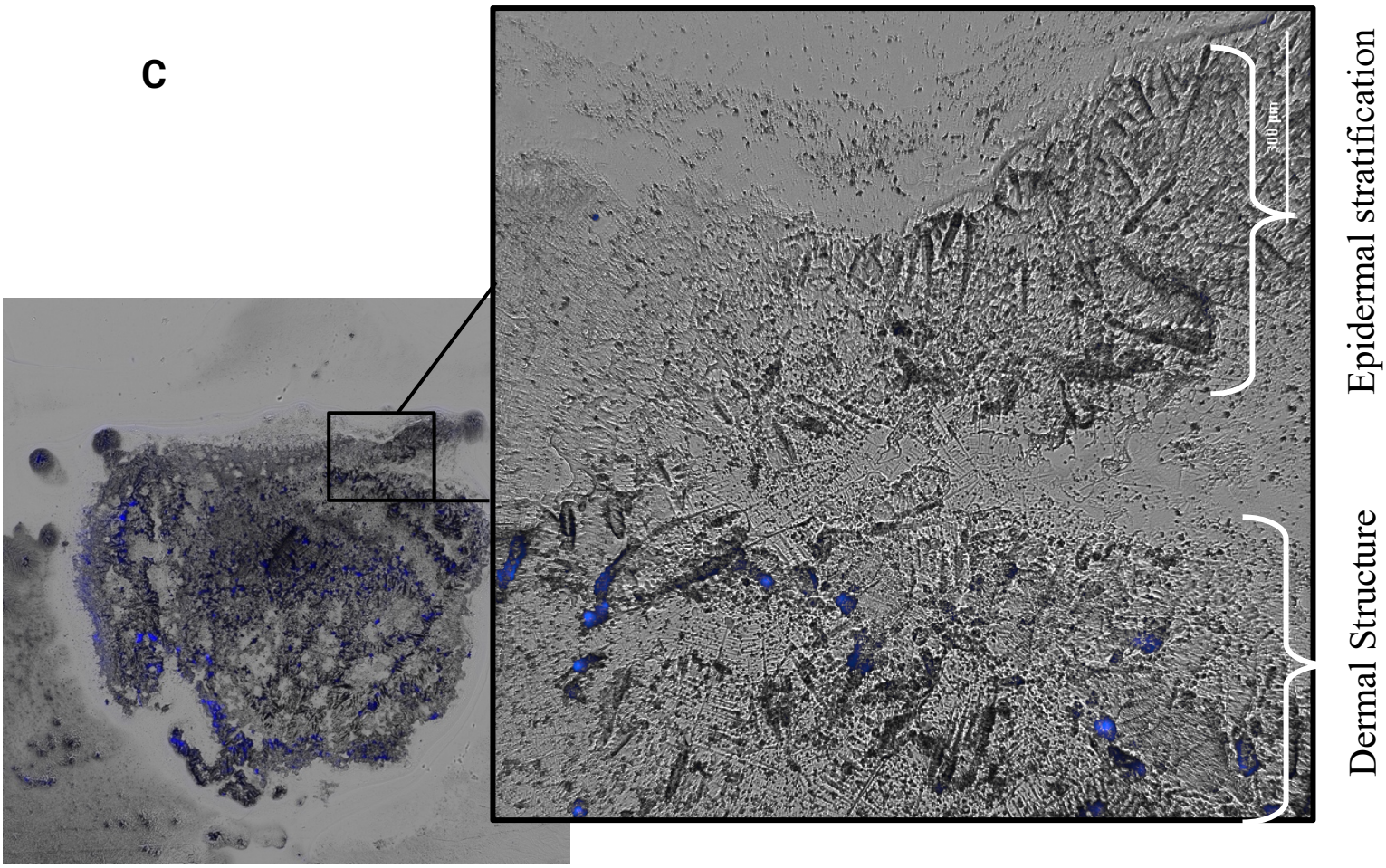

Figure 9. Fluorescence and brightfield evaluation of skin construct stratification and cellular distribution. (A) Control evaluation of an acellular construct imaged at 4X magnification. The DAPI channel displays the inherent autofluorescence of the natural biomaterials within the hydrogel matrix, while the brightfield and merge images establish the baseline scaffold morphology without cellular presence. **(B)** Analysis of the cellular 3D bioprinted construct showing successful epidermal development. DAPI staining confirms high cell density in the lower layers, with blue fluorescence indicating nuclear DNA. **(C)** High-magnification (20X) merge of the cellular construct illustrating terminal differentiation. The visualization reveals a distinct loss of fluorescence at the surface of the scaffold, corresponding to the formation of the stratum corneum (SC)**. This absence of DAPI signal confirms the presence of enucleated corneocytes, demonstrating that the refined printing parameters and ALI culture successfully replicated native human skin physiology.** *Scale bar:* 100 and 300 µm

3.2 Bioprocessing of the slices allow the visibility of the Stratum corneum formation and presence of the bacteria at the surface of the construct.

3.2.1 Synergistic microbiome interactions promote enhanced stratum corneum formation.

Safranin-O was employed as a structural marker to investigate the epidermal maturation within bioprinted constructs. The intense staining of the hydrogel scaffold is attributed to the ionic bonding between the cationic Safranin-O dye and the anionic carboxyl groups inherent in the alginate component of the bioink. More significantly, the distinct reddish-orange band observed at the scaffold surface confirms the successful development of a SC. This biological staining is driven by the dye's affinity for the negatively charged cholesterol sulfates and acidic natural moisturizing factors produced during the keratinocytes' terminal differentiation into corneocytes (Elias, 2012).

Brightfield microscopy at 20X magnification suggested that the SC thickness varied notably between the control and bacterial groups (Figure 10). To quantify these differences, a morphometric analysis was performed using Qupath 5.0. To ensure the data was representative and statically robust, eight measurements (N=8) were obtained for the experimental groups; control without bacteria, *S. epidermidis* monoculture and Co-infected. However, for the *S. aureus* monoculture group, four measurements (N=4) were performed. Furthermore, three representative histological slices analyzed from each of the three independent biological replicas (n= 3). The total area of the construct was manually annotated using the brush tool (highlighted with red). Meanwhile, the SC area was also manually annotated using the brush tool (highlighted with green), specifically targeting the cornified layer visible through the Safranin-O staining (Figure 11).

Moreover, taking into consideration varying slices sizes, the SC area was divided by the total area of the construct.

The results, visualized in the comparative graph in Figure 12, revealed significant structural changes in the barrier layer in response to the microbiome, where the three groups with inoculated bacteria; *S. aureus* monoculture, *S. epidermidis* monoculture and the co-infected group exhibited a statistically significant increase in SC thickness (****P <0.001) relative to the non-inoculated control (Motulsky., 2007). These findings demonstrate that the presence of microbial communities trigger a robust structural response, promoting a thicker SC in the bioprinted epidermis.

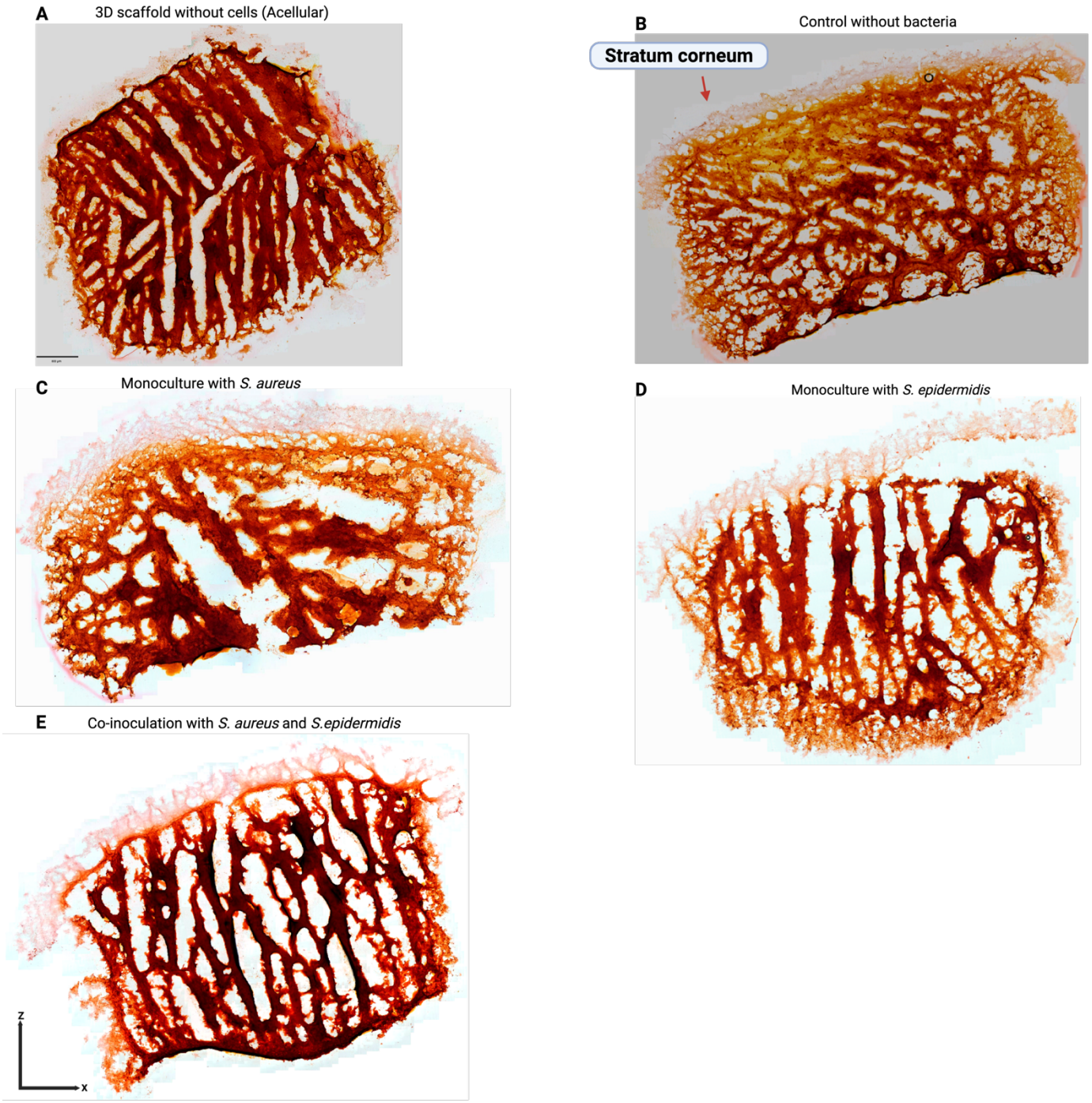

Figure 10. Qualitative histological evaluation of stratum corneum development via Safranin-O staining. Brightfield microscopy images (20X) of processed skin constructs across five experimental conditions: **(A) Acellular 3D scaffold, demonstrating a lack of surface development due to the absence of cellular activity; (B) Non-inoculated cellular control, showing initial epidermal barrier formation; (C) *Staphylococcus aureus* (*S. aureus*) monoculture, (D) *Staphylococcus epidermidis* (*S. epidermidis*) monoculture, and (E) Co-inoculation with *S. aureus* and *S. epidermidis*.** The reddish-orange band at the surface of cellular constructs (B-E) identifies the stratum corneum (SC), while the intense red staining of the internal matrix highlights the ionic interaction between the dye and the alginate-based hydrogel scaffold. Variation in the thickness and intensity of the SC band is visible between the non-inoculated control and microbial groups. *Scale bar:* 800 µm

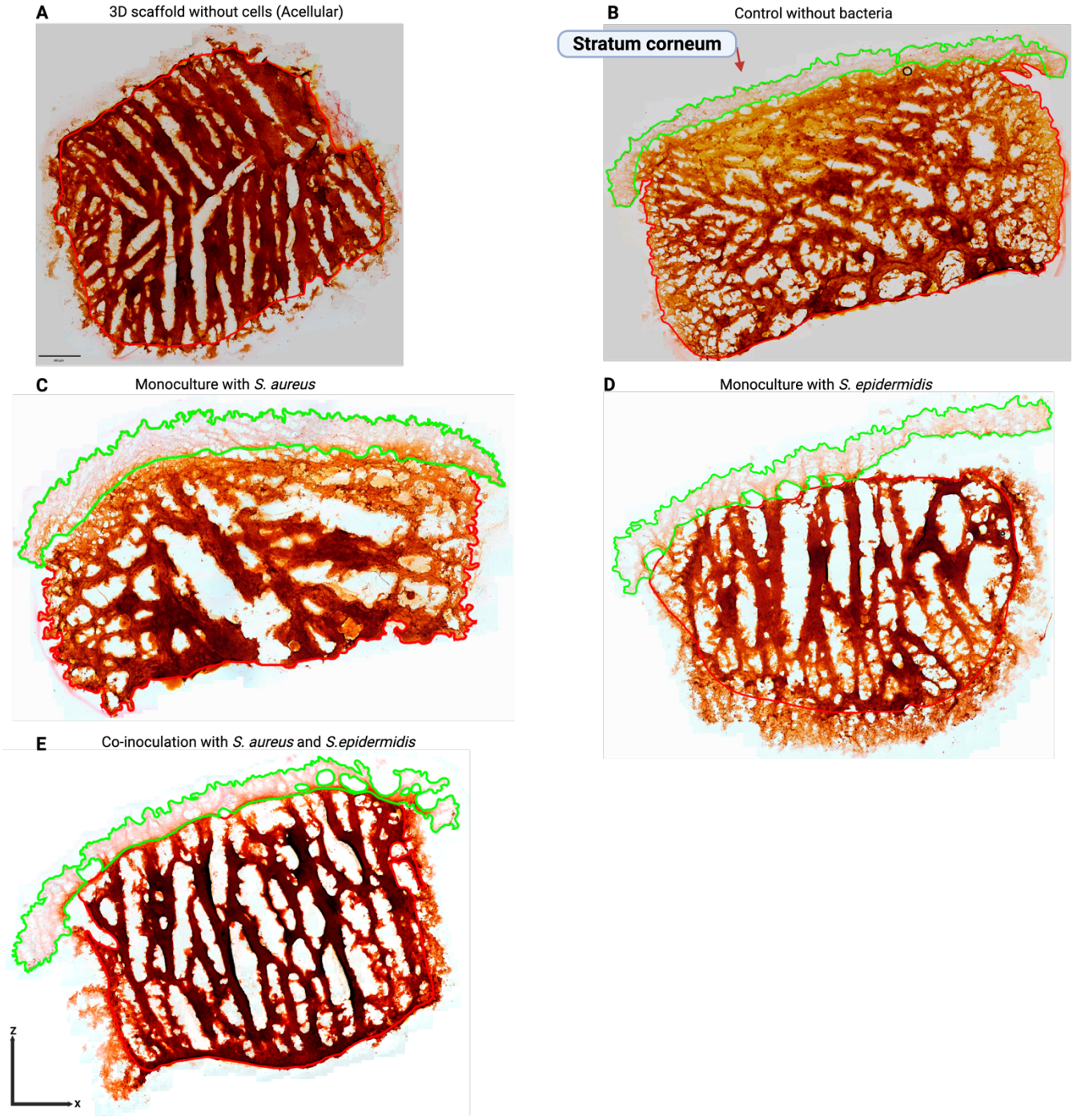

Figure 11. Morphometric analysis and area annotation of the cornified layer. Representative histological sections showing the quantitative measurement procedure with brush tool in QuPath 5.0 for the experimental groups: **(A) Acellular scaffold**, **(B) Control without bacteria**, **(C) *Staphylococcus aureus* (*S. aureus*) monoculture**, **(D) *Staphylococcus epidermidis* (*S. epidermidis*) monoculture**, and **(E) Co-inoculation**. The **green overlays** denote the **stratum corneum**, specifically targeting the reddish-orange cornified layer, while the **red outlines** define the total **construct area**. *Scale bar:* 800 µm

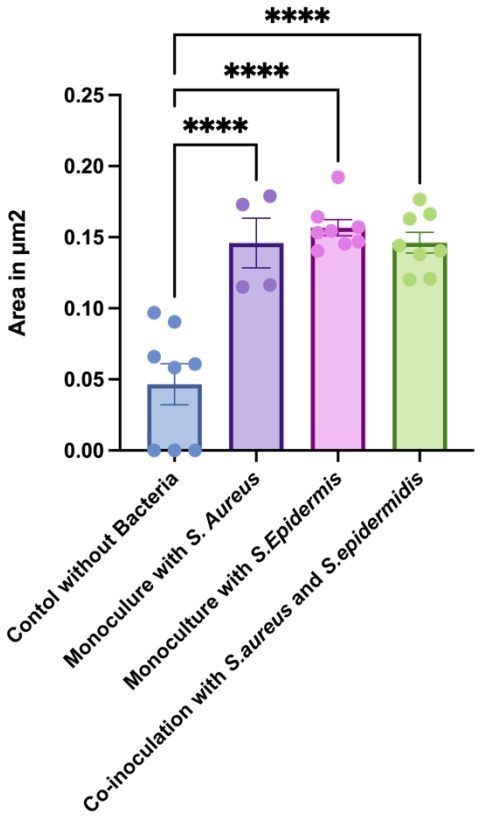

Figure 12. Statistical quantification of stratum corneum area in response to microbial inoculation. One-way ANOVA comparison of the **stratum corneum (SC) area** across experimental groups: Non-inoculated control (without Bacteria), *Staphylococcus aureus* (*S. aureus)* monoculture, *Staphylococcus epidermidis* (*S. epidermidis*) monoculture, and Co-infection. Prior to analysis, the data was confirmed to follow a **Gaussian distribution via the Shapiro-Wilk normality test, validating the use of parametric testing.** Bars represent the mean area with error bars indicating the standard error of the mean (SEM), and individual data points (*N=8* and *N*=4) are plotted to show the distribution across three independent biological replicates. The results demonstrate that the presence of microbial communities triggers a significant increase in SC area compared to the non-inoculated control. ***S. aureus*** monoculture, ***S. epidermidis*** monoculture and the **Co-infection** group exhibited an extremely significant increase in barrier thickness (****P < 0.001), **highlighting the synergistic effect of microbial presence on epidermal maturation**.

3.2.2 Spatial localization of the microbiome at surface of the construct.

To investigate the spatial distribution of the inoculated microbiota, Gram staining was employed as a structural marker to visualize the Gram-positive bacteria and confirm their presence at the scaffold surface. Histological slices from the four experimental groups; a Control without

bacteria, monoculture with *S. aureus*, monoculture with *S. epidermidis*, and a co-inoculation were evaluated using brightfield microscopy at 20X and 40X magnification.

Microscopic analysis revealed distinct purple-to-blue spherical clusters, characteristic of *S. aureus* and *S. epidermidis* morphology, localized at the surface of the scaffold in both the monoculture and co-infected groups. Figure 13 shows that these clusters were confined to the uppermost interface of the scaffold. In contrast, the non-inoculated control scaffolds showed no staining, confirming that no microbial clusters were present. These results demonstrated that the bacteria remained at the surface of the inoculated constructs, while the control group remained entirely free of microbial presence.

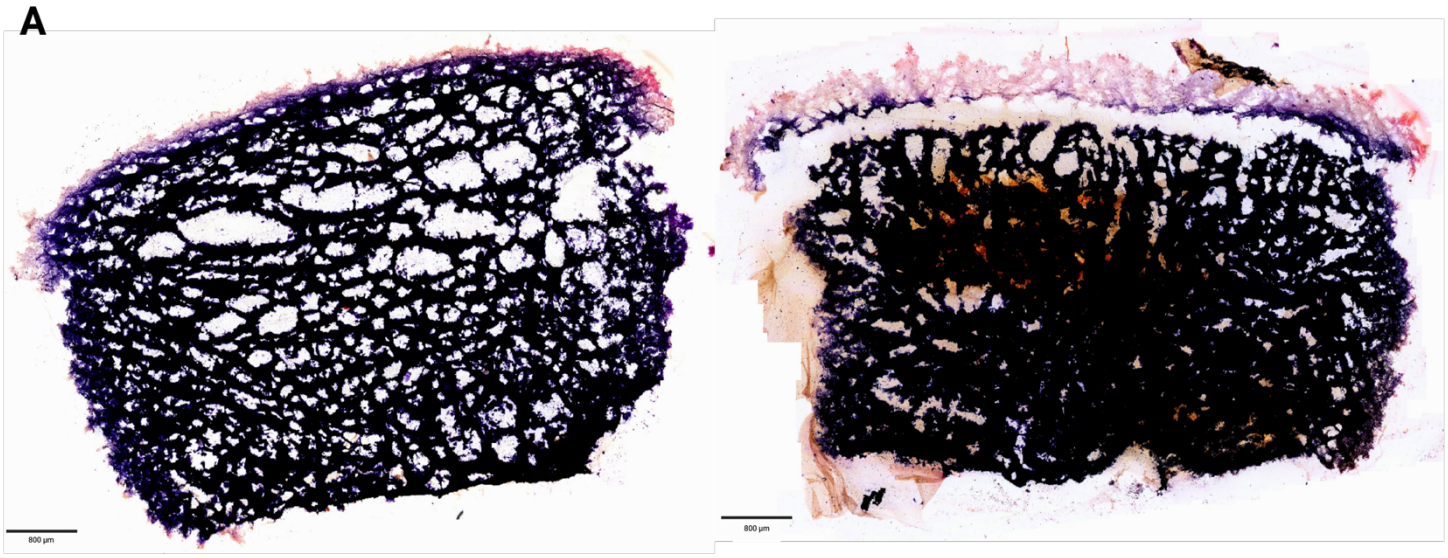

Control without bacteria

Monoculture with *S. aureus*

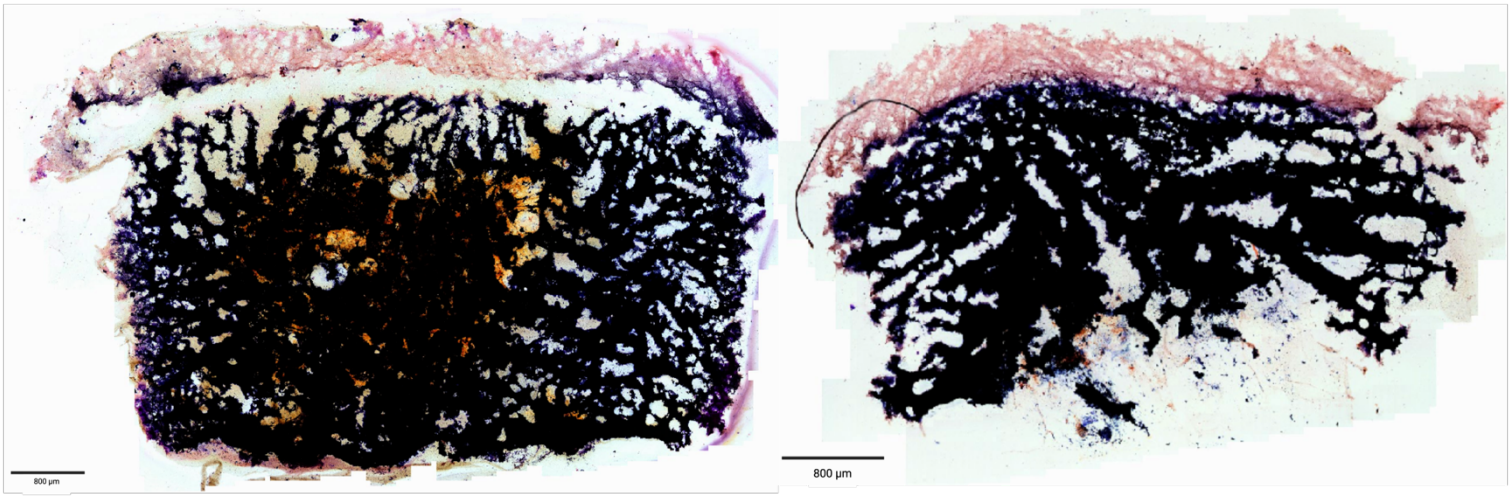

Monoculture with *S. epidermidis*

Co-inoculation with *S. aureus* and *S.epidermidis*

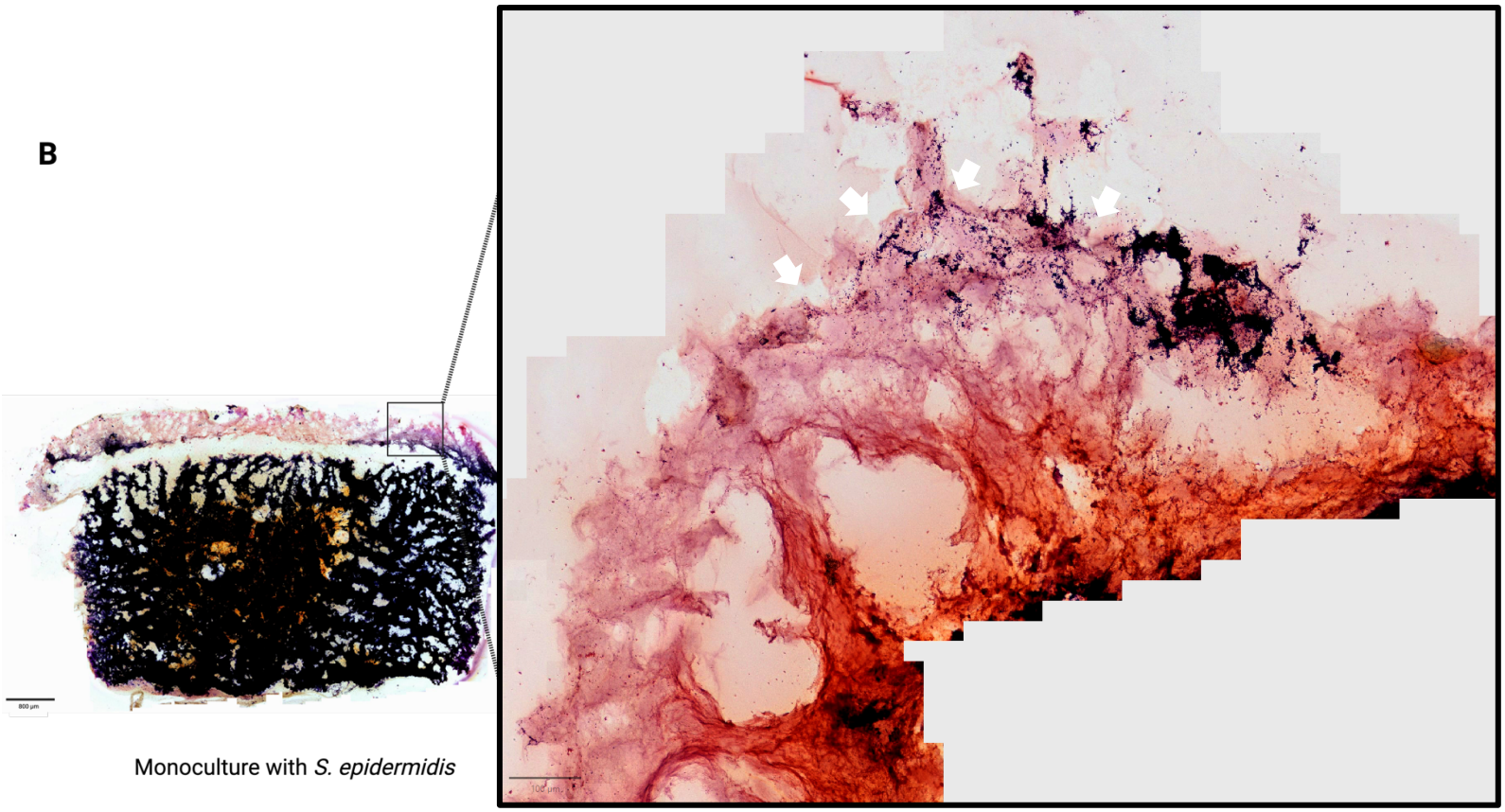

Figure 13. Gram staining for spatial distribution of the microbiome. (A) Brightfield microscopy images (20X) showing representative cross-sections of the four experimental groups. The non-inoculated control remains sterile, while the monoculture and co-infection groups display distinct purple-to-blue spherical clusters confined to the scaffold surface. **(B)** High-magnification magnified 40X view of the stratum corneum region of the slice with *Staphylococcus epidermidis* (*S.epidermidis*) monoculutre inoculation. White arrows indicate the presence of bacterial conglomerates with characteristic cocci morphology. These images confirm that the microbiome remains localized at the uppermost interface, successfully mimicking the spatial organization of native human skin. *Scale bar:* 800 and 100 µm

3.3 Host-Microbiome Immunological Interactions

Of the 48 cytokines, chemokines, and growth factors analyzed, 20 analytes fell within the validated standard curve sensitivity range (0.14 – 50.78 pg/mL). To evaluate the biological response to microbial presence, these analytes were subjected to statistical analysis using multiple paired t-tests. This approach compared the pre- and post-inoculation states within each of the four experimental groups: (control, *S. aureus* monoculture, *S. epidermidis* monoculture, and co-inoculation (refer to Tables 2, 3, 4, and 5 in the Appendix for detailed results).

As shown in Figure 14A, fibroblast growth factor (FGF) levels were higher across all groups post-inoculation. However, this increase is likely attributable to the fact that FGF is a primary component of the LSGS supplement utilized in the customized media. Since the culture media was refreshed during the inoculation process, these elevated levels may represent the detection of exogenous FGF rather than endogenous, cell-mediated signaling.

On the other hand, the *S. aureus* monoculture group exhibited a statistically significant increase in TGF- α (P=0.0081) following inoculation (Figure 14B). Furthermore, while statistically significant decreases were identified for Interlukin-3 (IL-3) (Figure 14C) and Granulocyte-macrophage colony-stimulating factor (GM-CSF) (P=0.0030) (Figure 14D) in the control group, and for TNF- α (P=0.044) in the co-infection group (Figure 14E) after inoculation, these changes represented marginal absolute differences at the edge of the assay's sensitivity limit (Refer to table 2 and 5). While these results reached the threshold for mathematical significance, their minimal magnitude suggests they represent a functional baseline rather than a robust biological transition (additional detected biomarkers lacking statistical significance are detailed in the Appendix).

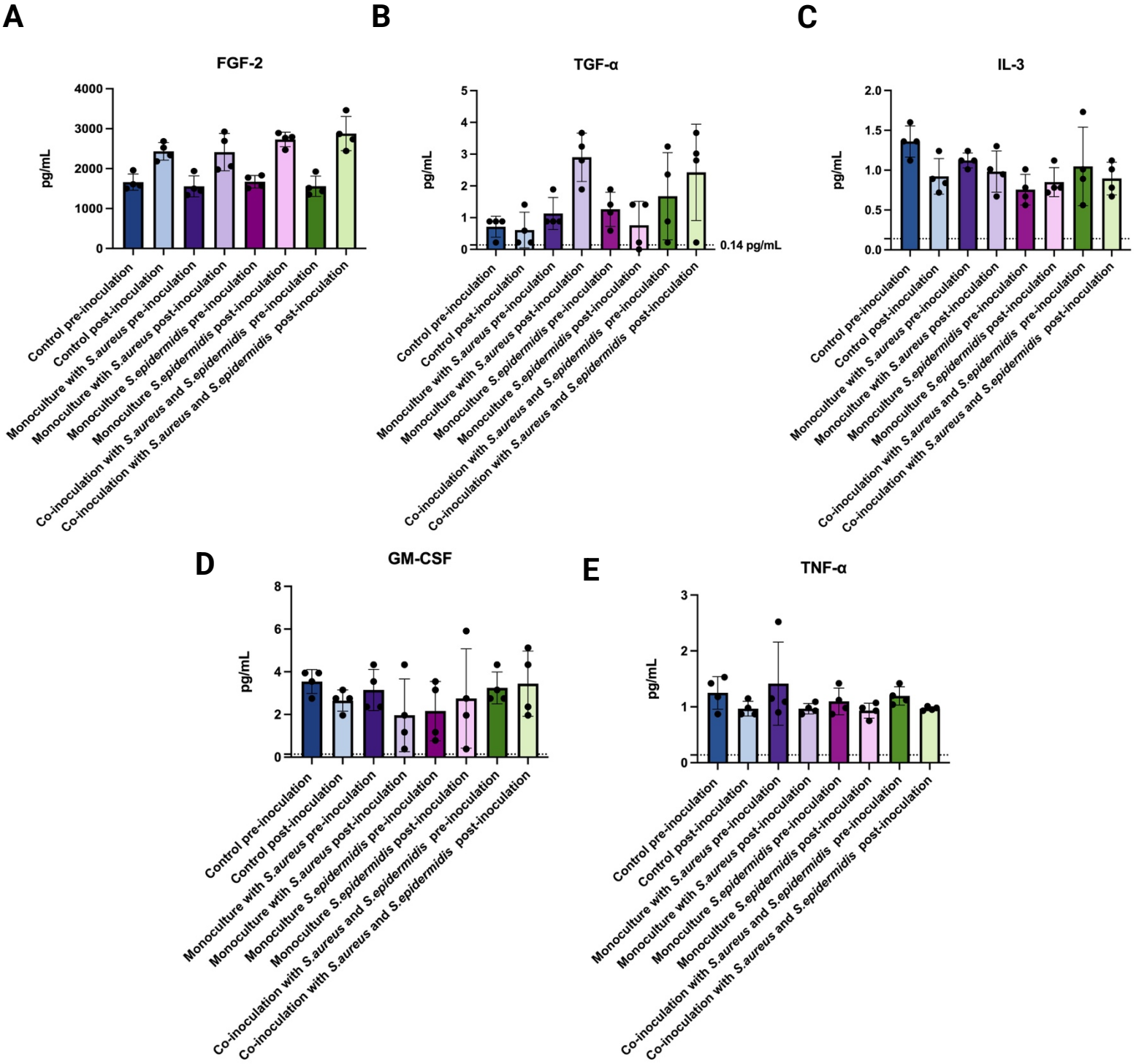

Figure 14. Cytokine, Chemokine and Growth Factor Profiling of the 3D Bioprinted Skin Model. (A) Fibroblast growth factor (FGF) levels increased across all groups post-inoculation, likely due to exogenous FGF-2 in the refreshed media. **(B)** Transforming Growth Factor- α (TGF-α) expression showed a significant increase (P=0.0081) in the *Staphylococcus aureus* (*S. aureus*) monoculture following inoculation. **(C)** Interlukin-3 (IL), **(D)** Granulocyte-macrophage colony-stimulating factor (GM-CSF) and **(E)** Tumor Necrosis Factor- α (TNF- α) exhibited statistically significant but marginal absolute shifts. While these analytes reached mathematical significance, their minimal magnitude indicates the signaling environment remained at a functional baseline (0.14 pg/mL). **Data represent mean ± SD of four biological replicates (*n*=4) per group; significance determined by multiple paired t-tests comparing pre- and post-inoculation states.**

CHAPTER 4- DISCUSSION

Our study investigated the development of a stratified, 3D bioprinted skin co-culture model using extrusion-based technology. By utilizing a high-viscosity fibrin hydrogel, we incorporated HDFs to mimic the dermal layer and HEKa to recreate the epidermis. Stratification was achieved by transitioning the scaffold from an embedded culture to the ALI culture methodology, which resulted in an epidermal barrier that resembled native skin. We established a functional model to explore pathological host-microbe interactions. This demonstrated the ability to maintain human microbiome bacteria, specifically *S. epidermidis* and *S. aureus*, on the scaffold surface. To support these findings, we optimized histological protocols by adapting traditional techniques for tissue-engineered constructs. This allowed for the clear visualization of scaffold arrangements, bacterial localization, and, crucially, the confirmation of successful SC formation. Furthermore, through biochemical tracking via cytokine profiling, we evaluated the intracellular signaling between cutaneous cells and microorganisms within the model.

We began by analyzing the importance of the 3D co-culture construct and specific bioprinting features to optimize communication between cutaneous cells. These interactions are fundamental for scaffold maintenance and SC formation; as noted in previous literature, co-cultures exhibit superior proliferation and maturation kinetics compared to monoculture models (Andrade et al., 2025). To enhance cellular crosstalk and improve structural alignment for stratification, we refined the internal architecture by transitioning from a 30% infill honeycomb pattern to a 65% infill rectilinear pattern. This optimization provided the mechanical stability required to support the ALI and subsequent microbial inoculation.

Building upon this structural foundation, we examined the complexity of SC formation within the high-viscosity fibrin hydrogel. The transition to ALI facilitated the exposure of cells to

atmospheric O_2, shifting the environment from relatively hypoxic submerged conditions toward hyperbaric conditions. This transition significantly increased SC thickness by triggering a metabolic shift from glycolysis to mitochondrial metabolism, which is essential for the terminal differentiation of keratinocytes into a durable protective barrier (Chettouh-Hammas et al., 2024).

To validate this maturation and microbiome colonization, it was necessary to overcome the technical challenges of analyzing a water-rich polymeric hydrogel. Traditional paraffin embedding involves ethanol-based dehydration, which often causes hydrogel collapse and incomplete wax infiltration (Ragauskas et al., 2025). Consequently, we optimized a cryohistological procedure using intercalating ratios of sucrose gradients (5% and 30%) and O.C.T compound. As noted by Xie *et al*., sucrose regulates the shape and delays the growth of ice crystals through recrystallization inhibition, while gradual O.C.T addition improves sectioning quality and maintains low background standards (Ruan et al., 2013). This optimized cryopreservation protocol successfully displaced internal water to minimize ice crystal formation, preserving the structural and cellular integrity of the high-viscosity fibrin scaffolds and allowing for high-resolution histological analysis typically difficult in 3D constructs.

Histological validation began with H&E staining. While H&E was helpful for evaluating different infills to achieve correct alignment, the hydrogel matrix exhibited characteristic non-specific purple staining. Unlike traditional models where the epidermis and dermis show distinct coloration (Liu et al., 2024), our high-viscosity bioink functioned as a "nucleus-like" hydrogel. This occurred because genipin reacts with fibrin amino acids to create dark-blue pigments, while the high density of carboxyl groups in the alginate mimics the negative charge of DNA, causing hematoxylin to bind to the entire matrix. To overcome this issue, DAPI fluorescent staining was employed to distinguish between living epidermal layers and the dead barrier. The distinct absence

of fluorescence in the uppermost part of the construct confirmed the presence of acellular, enucleated corneocytes, verifying the successful transition of keratinocytes into a cornified barrier (Hermsmeier et al., 2018).

Furthermore, Safranin-O staining served as a structural marker to evaluate the extracellular matrix and quantify barrier thickness. In this context, Safranin-O targets acidic glycosaminoglycans and the anionic carboxyl groups of the alginate, visualizing the "synthetic ECM" supporting the cells. In terms of skin maturation, Safranin-O marks the biological ECM by binding to cholesterol sulfates and acidic natural moisturizing factors produced during terminal differentiation (Elias, 2012). Morphometric analysis of these stained slices revealed that the microbiome actively promoted barrier maturation. Specifically, *S. epidermidis* monocultures and co-infections showed a statistically significant increase in SC area and thickness compared to non-inoculated controls (****$P<0.001$). Furthermore, the *S. aureus* monoculture also showed a significant increase in SC area. However, because of the small sample size, these measurements are not enough to prove a statistically significant result. Therefore, an area of improvement for future studies is to use a larger sample size.

This biological significance underscores that the microbiome is not a passive resident but an active participant in skin maturation. As established by Zheng *et al*., *S. epidermidis* maintains a symbiotic relationship with the host by secreting sphingomyelinase, an enzyme nearly omnipresent across the species. This microbial Sph enzyme catalyzes the cleavage of sphingomyelin into two essential products: ceramides and phosphocholine (PC). While the host produces its own endogenous acid sphingomyelinase (aSMase), microbial Sph acts as a potent supplementary catalyst. This interaction represents a metabolic synergy: the microorganism boosts the production of ceramides, which constitute over 50% of the SC lipid matrix, thereby reinforcing barrier

integrity. In return, the PC generated provides a vital source of carbon and nitrogen for the bacteria and serves as a precursor for osmoprotectants, which are essential for *S. epidermidis* survival in the acidic environment of the skin. Consequently, the statistically significant increase in SC thickness observed in our *S. epidermidis* and co-infected constructs suggests that the bacteria effectively "prime" and reinforce the primary air-liquid barrier through this synergistic metabolic collaboration (Zheng et al., 2022a).

Crucially, Gram staining was fundamental for characterizing the inoculated bacteria and confirming their spatial localization within the model. This technique relies on the structural differences in bacterial cell walls; specifically, the thick peptidoglycan layer of the Gram-positive cell membrane in *S. aureus* and *S. epidermidis* retains the crystal violet-iodine complex, resulting in a distinct purple-to-blue coloration even after decolorization (Javaeed et al., 2021). Microscopic analysis revealed these characteristic spherical clusters localized strictly at the uppermost interface of the scaffold. This confirms that the bacteria remained at the surface where they naturally reside in human skin, rather than infiltrating the deeper hydrogel layers (Díaz et al., 2025).

Finally, through the biochemical tracking via cytokine profiling, we step forward to understand the intracellular crosstalk between the host and their commensals within the *in vitro* model. Growth factors such as, VEGF-A and TGF-α were detected; these are both continuously produced and released by keratinocytes to drive tissue maintenance (Satapathy et al., 2025). VEGF-A acts as an essential promigratory meditator, responsible for the transition of cells from the deep basal layer upward through the upper layers. This vertical movement is a central component of the skin's continuous renewal, allowing the epidermis to constantly re-establish the protective barrier and maintain a functional stratum corneum (Maksimoska et al., 2025). Simultaneously, TGF-α functions on the Epidermal growth factor (EGF) receptor to augment both

keratinocyte migration and proliferation. By serving as a potent trigger for the division of cells in the basal layer, ensuring a steady supply of new keratinocytes that can eventually differentiate and move toward the surface to sustain the skin's structural integrity (Satapathy et al., 2025; Tito et al., 2025).

Therefore, having a significant increase of the TGF-α after inoculation on the group's monoculture with *S. aureus* and co-infected supports the hypothesis that the keratinocytes are stimulated by the microorganisms to release growth factors as part of an early immune and regenerative response. Subsequently, as a potent ligand for the EGF receptor, TGF-α triggers the proliferation of cells in the basal layer and augment their migration upon the surface of the construct. This coordinated movement is essential for re-epithelization and to re-establish the protective SC (Morán et al., 2013; Tito et al., 2025).

Furthermore, the downward fluctuation of GM-CSF, IL-3 and TNF- α, and other cytokines from their functional baseline post-inoculation suggested an inflammatory mediation that prevented a dysregulated immune cells activation (Lee et al., 2022; Satapathy et al., 2025; Volksdorf et al., 2018). These findings indicated that there was a host-microbiome crosstalk aimed at maintaining a homeostatic microenvironment and epidermal barrier function.

In accordance with the established understanding of the skin as a co-dependent ecosystem, host cells and their resident microbiome function in a bidirectional partnership. Through this interlinked communication, immune activity is modulated and the cutaneous barrier is maintained; in exchange, the host provides the vital source of nutrients and the structural enviroment necessary for these microorganisms to inhabit and thrive (Lee et al., 2022; Zheng et al., 2022). We developed a 3D skin model that mimics the lipid-rich architecture of the SC. This provides the specific surface

required for microorganisms to reside and engage in the functional crosstalk that actively promotes the epidermal maturation (Díaz et al., 2025; Holland et al., 2002; Wang et al., 2025).

CHAPTER 5- CONCLUSION AND FUTURE WORK

The 3D bioprinted skin model presented in this work offers significant advantages over existing *in vitro* platforms by successfully replicating the complex, multi-layered architecture of human skin. By incorporating primary human keratinocytes and fibroblasts, the model facilitates essential epithelial-mesenchymal crosstalk, which is fundamental for both scaffold maintenance and ECM production. This inherent cellular signaling, combined with the ALI culture methodology, provided the necessary physiological cues to drive the terminal differentiation and organized stratification of the epidermis (Madison et al., 1988; Sun et al., 2024).

As a result of this maturation, the SC, the skin's outermost layer and primary barrier, was successfully developed. Beyond acting as a physical, chemical, and immunological shield, the SC was demonstrated to be the critical enucleated site where host-microbe collaboration is established. It is within this specialized niche that the microbiome resides, maintaining a homeostatic balance that is vital for preventing pathogenic infiltration and regulating transepidermal water loss (Krieken et al., 2016; Stefanovic et al., 2024).

The fabrication of these constructs was achieved through EBB, a robust and versatile technique that allowed for the production capacity of at least 15 individual constructs. Through this method, rapid and effective optimization of printing features, such as dimensions, infill density, and specific deposition patterns, was achieved. This provided the precision needed to develop complex models with interconnected cell populations in a single session and enabled the creation of a solid, stable platform with sufficient structural integrity to support the microbiome

without the need for invasive inoculation methods. In contrast to the previous model iterations described in Díaz *et al*, where bacteria were directly injected into the scaffold (Díaz et al., 2025). The current platform enables microbial inoculation onto the tissue surface, thereby more accurately replicating the natural colonization process of human skin.

A core objective of this research was to streamline and enhance the analysis of 3D hydrogels, addressing the inherent difficulties associated with the visual characterization of three-dimensional structures due to their opacity. By adapting globally accepted histological techniques, a cryopreservation procedure was optimized to displace internal hydrogel water and prevent ice crystal formation, thereby preserving the structural and cellular integrity of the high-viscosity fibrin scaffolds (Ruan et al., 2013). This enabled high-resolution histological analyses, including Gram, Safranin-O, and H&E staining, as well as DAPI immunofluorescence. These tools allowed for the verification of the SC and validated the model's efficacy as a colonization platform. Specifically, it was confirmed that the inoculated microbiota localized strictly within the upper interface of the SC, accurately mimicking the spatial distribution found in native human skin.

Furthermore, the results confirmed a metabolic synergy between the host and the microbiota. It was observed that constructs with an active microbiome exhibited more robust SC development; notably, those colonized with *S. epidermidis*, or co-infected communities resulted in a significantly thicker SC. This aligned with literature stating that *S. epidermidis* boosts ceramide production, which constitutes over 50% of the SC lipid matrix (Zheng et al., 2022).

Moreover, the detection of growth factors such as VEGF-A and TGF-α was significant, as they served as central mediators for keratinocyte migration and proliferation. These are essential factors for the skin's continuous renewal, allowing the epidermis to constantly re-establish the cutaneous barrier (Satapathy et al., 2025). Specifically, the increase in TGF-α following *S. aureus*

and co-inoculated treatments lined up with the hypothesis that host cells were stimulated by the microorganisms to release growth factors as part of an early immune regenerative response (Morán et al., 2013). Subsequently, the fact that other cytokines levels remained at a functional baseline, showing a downward fluctuation post-inoculation, suggested that inflammatory mediation occurred, thereby avoiding a dysregulated immune cell activation. This confirmed a functional crosstalk between the host and the microbiome, where they interacted synergistically to maintain a homeostatic microenvironment and maintain the epidermal barrier functions (Liu et al., 2023).

Despite these advancements, a primary limitation resides in the choice of bioink. While fibrin is a natural constituent of the skin's ECM, its inherent reactivity causes non-specific staining during histological analysis, which can obscure tissue boundaries and complicate precise visualization. More importantly, its susceptibility to staphylokinase-mediated fibrinolysis by *S. aureus* presents a significant challenge; the pathogen utilizes fibrin for sequestration before enzymatic dissolution, compromising the long-term structural integrity of the construct (Thomas et al., 2019).

Consequently, future iterations should incorporate Type I Collagen, which constitutes 90% of the native human dermis. Beyond providing superior mechanical realism, collagen is essential for the next stage of model complexity: vascularization (Chhum et al., 2016; Shi et al., 2023). Its bioactive properties provide the necessary ligands for endothelial cell attachment and migration, serving as the biological template for developing a functional capillary network. The integration of a vascular component, alongside the addition of the upper hair follicle (uHF) for sebum production and immune signaling, would transform this framework into a truly holistic representation of human physiology (Ford et al., 2024). Finally, while Gram staining confirmed bacterial localization, the current lack of Colony Forming Unit (CFU) quantification limits the

ability to statistically prove the competitive inhibition of *S. aureus*. Future work should include CFU assays to quantitatively evaluate these microbe-microbe interactions (Díaz et al., 2025).

Ultimately, this research establishes a more realistic and physiologically accurate platform that reflects the complexity of human skin by accounting for the inherent microbiome and its synergistic interaction with cutaneous cells. This provides a robust model for the in-depth study of these biological interactions, specifically regarding how the immune response is triggered and how the collaboration between the microbiome and skin cells establishes early homeostasis during the initial stages of wound healing. By acknowledging and understanding these interactions, advanced therapies can be developed to restore homeostasis, control pathogen proliferation, and interrupt the "vicious cycle" of inflammation. This comprehensive approach provides a crucial standardization for the creation and analysis of 3D skin models, democratizing additive manufacturing while fostering more efficient innovation for future tissue engineering.

APPENDIX

Table 2. Statistical analysis of cytokine and growth factor expression in the Control group (Pre- vs. Post-Inoculation).

Cytokines/ Chemokines	Below Threshold ?	P value	*Control pre-inoculated*	*Control post-inoculated*	Difference	SE of difference
EGF	No	0.536239	10965	15720	-4755	6827
Eotaxin	No	0.428586	5.61	6.078	-0.4675	0.5121
FGF-2	Yes	0.000991	1661	2432	-770.8	59.45
FLT-3L	No	0.125588	0.92	0.6175	0.3025	0.1435
GM-CSF	Yes	0.002992	3.543	2.653	0.89	0.1
GROα	No	0.25554	228.1	84.96	143.1	102.1
IL-1α	No	0.153539	3.178	0.48	2.698	1.419
IL-3	Yes	0.001168	1.36	0.9225	0.4375	0.03568
IL-5	No	0.154619	0.1225	0.0875	0.035	0.01848
IL-6	No	0.184595	131.7	29.46	102.2	59.55
IL-7	No	0.287253	0.76	0.945	-0.185	0.1433
IL-8	No	0.168526	611.1	202.4	408.7	226.2
IL-17E/IL-25	No	0.385566	9.075	7.885	1.19	1.174
M-CSF	No	0.167483	49.71	16.97	32.73	18.05
MCP-1	No	0.305922	493	276.9	216	175.4
MDC	No	0.686494	0.5275	0.57	-0.0425	0.09551
TGFα	No	0.765843	0.715	0.61	0.105	0.3221
TNFα	No	0.1775	1.25	0.9675	0.2825	0.161
TNFβ	No	0.74258	1.408	1.633	-0.225	0.6247
VEGF-A	No	0.055876	5.438	4.243	1.195	0.3931

Table 3. Statistical analysis of cytokine and growth factor expression in the monoculture *S.aureus* group (Pre- vs. Post-Inoculation).

Cytokines/ Chemokines	Below Threshold ?	P value	*S.aureus pre-inoculation*	*S.aureus post-inoculation*	Difference	SE of difference
EGF	No	0.281918	6199	8349	-2150	1643
Eotaxin	No	0.127575	5.403	6.078	-0.675	0.3227
FGF-2	Yes	0.02869	1555	2413	-857.4	216.3
FLT-3L	No	0.080913	0.7025	0.5625	0.14	0.05401
GM-CSF	No	0.133739	3.148	1.96	1.188	0.5814
GROα	No	0.26943	295.6	27.22	268.4	198.6
IL-1α	No	0.178078	2.938	0.955	1.983	1.132
IL-3	No	0.484413	1.123	0.9825	0.14	0.176
IL-5	No	0.604181	0.105	0.1	0.005	0.00866
IL-6	No	0.287501	211.7	39.12	172.6	133.8
IL-7	No	0.054981	0.9275	1.165	-0.2375	0.07761
IL-8	No	0.267334	973.3	127.8	845.5	622.2
IL-17E/IL-25	No	0.979949	9.045	9.075	-0.03	1.1
M-CSF	No	0.108427	74.4	15.58	58.82	25.97
MCP-1	No	0.222875	511.8	123.7	388.1	253.2
MDC	No	0.154607	0.5375	0.43	0.1075	0.05677
TGFα	Yes	0.008125	1.133	2.9	-1.768	0.2811
TNFα	No	0.307896	1.415	0.9675	0.4475	0.3652
TNFβ	No	0.667174	1.338	1	0.3375	0.7104
VEGF-A	No	0.508101	4.9	3.938	0.9625	1.285

Table 4. Statistical analysis of cytokine and growth factor expression in the monoculture *S.epidermidis* group (Pre- vs. Post-Inoculation).

Cytokines/ Chemokines	Below Threshold ?	P value	*S.epidermidis pre-inoculation*	*S.epidermidis post-inoculation*	Difference	SE of difference
EGF	No	0.407062	13902	10308	3594	3736
Eotaxin	No	0.400981	5.063	5.5	-0.4375	0.4482
FGF-2	Yes	0.000988	1671	2730	-1059	81.61
FLT-3L	No	0.889086	0.59	0.62	-0.03	0.1978
GM-CSF	No	0.587344	2.16	2.75	-0.59	0.9737
GROα	No	0.262207	43.97	10.07	33.9	24.61
IL-1α	No	0.331355	43.23	1.36	41.87	36.21
IL-3	No	0.198846	0.755	0.85	-0.095	0.05781
IL-5	No	0.296689	0.0825	0.0975	-0.015	0.0119
IL-6	No	0.284844	67.06	18.27	48.79	37.57
IL-7	No	0.435351	0.7125	0.7875	-0.075	0.08352
IL-8	No	0.298298	301.9	74.6	227.3	181.1
IL-17E/IL-25	No	0.826446	8.69	8.5	0.19	0.7947
M-CSF	No	0.149366	27.3	6.725	20.58	10.67
MCP-1	No	0.23786	120.8	44.7	76.06	51.73
MDC	No	0.390525	0.5875	0.5025	0.085	0.0849
TGFα	No	0.081149	1.263	0.76	0.5025	0.1941
TNFα	No	0.083678	1.098	0.9325	0.165	0.06461
TNFβ	No	0.073197	1.768	1.045	0.7225	0.2667
VEGF-A	No	0.847028	3.838	3.89	-0.0525	0.2498

Table 5. Statistical analysis of cytokine and growth factor expression in the co-infected (*S.epidermidis* and *S. aureus*) group (Pre- vs. Post-Inoculation).

Cytokines/ Chemokines	Below Threshold ?	P value	*Co-infected pre-inoculation*	*Co-infected post-inoculation*	Difference	SE of difference
EGF	No	0.871609	8591	8153	438.3	2492
Eotaxin	No	0.376699	4.68	6.078	-1.398	1.35
FGF-2	Yes	0.002642	1557	2877	-1320	142.2
FLT-3L	No	0.226979	0.5925	0.8875	-0.295	0.1947
GM-CSF	No	0.808781	3.245	3.443	-0.1975	0.7477
GROα	No	0.263626	49.32	18.59	30.72	22.39
IL-1α	No	0.063561	5.86	1.785	4.075	1.415
IL-3	No	0.649919	1.048	0.895	0.1525	0.3035
IL-5	No	0.367198	0.0925	0.11	-0.0175	0.01652
IL-6	No	0.257554	68.11	23	45.11	32.36
IL-7	No	0.166888	0.6825	0.7925	-0.11	0.06055
IL-8	No	0.260016	361.1	122.9	238.2	171.9
IL-17E/IL-25	No	0.179154	8.48	6.713	1.768	1.012
M-CSF	No	0.387263	13.35	9.108	4.238	4.199
MCP-1	No	0.29047	75.33	36.68	38.65	30.19
MDC	No	0.689192	0.4975	0.4475	0.05	0.1134
TGFα	No	0.536483	1.675	2.428	-0.7525	1.081
TNFα	Yes	0.043993	1.195	0.9675	0.2275	0.06787
TNFβ	No	0.92387	1.273	1.18	0.0925	0.891
VEGF-A	No	0.071398	4.025	3.843	0.1825	0.06663

REFERENCES

Ali, N., Zirak, B., Rodriguez, R. S., Pauli, M. L., Truong, H.-A., Lai, K., Ahn, R., Corbin, K., Lowe, M. M., Scharschmidt, T. C., Taravati, K., Tan, M. R., Ricardo-Gonzalez, R. R., Nosbaum, A., Bertolini, M., Liao, W., Nestle, F. O., Paus, R., Cotsarelis, G., … Rosenblum, M. D. (2017). Regulatory T Cells in Skin Facilitate Epithelial Stem Cell Differentiation. *Cell*, *169*(6), 1119-1129.e11. https://doi.org/10.1016/j.cell.2017.05.002

Andrade, T. A. M., Da Silva, V. A., Scheck, K., Garay, T., Sharma, R., & Willerth, S. M. (2025). 3D Bioprinting a Novel Skin Co-Culture Model Using Human Keratinocytes and Fibroblasts. *Journal of Biomedical Materials Research Part A*, *113*(1), e37831. https://doi.org/10.1002/jbm.a.37831

Aydin, L., Kucuk, S., & Kenar, H. (2020). A universal self-eroding sacrificial bioink that enables bioprinting at room temperature. *Polymers for Advanced Technologies*, *31*(7), 1634–1647. https://doi.org/10.1002/pat.4892

Bankhead, P., Loughrey, M. B., Fernández, J. A., Dombrowski, Y., McArt, D. G., Dunne, P. D., McQuaid, S., Gray, R. T., Murray, L. J., Coleman, H. G., James, J. A., Salto-Tellez, M., & Hamilton, P. W. (2017). QuPath: Open-source software for digital pathology image analysis. *Scientific Reports*, *7*(1), 16878. https://doi.org/10.1038/s41598-017-17204-5

Boularaoui, S., Al Hussein, G., Khan, K. A., Christoforou, N., & Stefanini, C. (2020). An overview of extrusion-based bioprinting with a focus on induced shear stress and its effect on cell viability. *Bioprinting*, *20*, e00093. https://doi.org/10.1016/j.bprint.2020.e00093

Brown, T. M., & Krishnamurthy, K. (2025). Histology, Dermis. In *StatPearls*. StatPearls Publishing. http://www.ncbi.nlm.nih.gov/books/NBK535346/

Chabi, R., & Momtaz, H. (2019). Virulence factors and antibiotic resistance properties of the Staphylococcus epidermidis strains isolated from hospital infections in Ahvaz, Iran. *Tropical Medicine and Health*, *47*(1), 56. https://doi.org/10.1186/s41182-019-0180-7

Chen, X. B., Fazel Anvari-Yazdi, A., Duan, X., Zimmerling, A., Gharraei, R., Sharma, N. K., Sweilem, S., & Ning, L. (2023). Biomaterials / bioinks and extrusion bioprinting. *Bioactive Materials*, *28*, 511–536. https://doi.org/10.1016/j.bioactmat.2023.06.006

Chettouh-Hammas, N., & Grillon, C. (2024). Physiological skin oxygen levels: An important criterion for skin cell functionality and therapeutic approaches. *Free Radical Biology and Medicine*, *222*, 259–274. https://doi.org/10.1016/j.freeradbiomed.2024.06.015

Chhum, P., Yu, H., An, B., Doyon, B. R., Lin, Y.-S., & Brodsky, B. (2016). Consequences of Glycine Mutations in the Fibronectin-binding Sequence of Collagen. *Journal of Biological Chemistry*, *291*(53), 27073–27086. https://doi.org/10.1074/jbc.M116.753566

Chrenek, J., Kirsch, R., Scheck, K., & Willerth, S. M. (2022). Protocol for printing 3D neural tissues using the BIO X equipped with a pneumatic printhead. *STAR Protocols*, *3*(2), 101348. https://doi.org/10.1016/j.xpro.2022.101348

Christensen, G. D., Simpson, W. A., Bisno, A. L., & Beachey, E. H. (1982). Adherence of slime-producing strains of Staphylococcus epidermidis to smooth surfaces. *Infection and Immunity*, *37*(1), 318–326. https://doi.org/10.1128/iai.37.1.318-326.1982

Chudnovskiy, A., Pasqual, G., & Victora, G. D. (2019). Studying interactions between dendritic cells and T cells in vivo. *Current Opinion in Immunology*, *58*, 24–30. https://doi.org/10.1016/j.coi.2019.02.002

Conwill, A., Kuan, A. C., Damerla, R., Poret, A. J., Baker, J. S., Tripp, A. D., Alm, E. J., & Lieberman, T. D. (2022). Anatomy promotes neutral coexistence of strains in the human skin microbiome. *Cell Host & Microbe*, *30*(2), 171-182.e7. https://doi.org/10.1016/j.chom.2021.12.007

Derman, I. D., Rivera, T., Garriga Cerda, L., Singh, Y. P., Saini, S., Abaci, H. E., & Ozbolat, I. T. (2024). Advancements in 3D skin bioprinting: Processes, bioinks, applications and sensor integration. *International Journal of Extreme Manufacturing*, *7*(1), 012009. https://doi.org/10.1088/2631-7990/ad878c

Derr, K., Zou, J., Luo, K., Song, M. J., Sittampalam, G. S., Zhou, C., Michael, S., Ferrer, M., & Derr, P. (2019). Fully Three-Dimensional Bioprinted Skin Equivalent Constructs with Validated Morphology and Barrier Function. *Tissue Engineering Part C: Methods*, *25*(6), 334–343. https://doi.org/10.1089/ten.tec.2018.0318

Díaz, G., Perry, M., Cárdenas, L., Da Silva, V., Scheck, K., Tschofen, S., Tuffs, S., & Willerth, S. (2025). Protocol for 3D Bioprinting a Co-culture Skin Model Using a Natural Fibrin-Based Bioink as an Infection Model. *BIO-PROTOCOL*, *15*(1376). https://doi.org/10.21769/BioProtoc.5380

Díaz, G. Y., Da Silva, V. A., Kalantarnia, F., Scheck, K., Tschofen, S. A., Tuffs, S. W., & Willerth, S. M. (2025). Using Three-Dimensional Bioprinting to Generate Realistic Models of

Wound Healing. *Advances in Wound Care*, wound.2024.0138. https://doi.org/10.1089/wound.2024.0138

Dreifke, M. B., Jayasuriya, A. A., & Jayasuriya, A. C. (2015). Current wound healing procedures and potential care. *Materials Science and Engineering: C*, *48*, 651–662. https://doi.org/10.1016/j.msec.2014.12.068

Dwivedi, A., Agarwal, N., Ray, L., & Tripathi, A. K. (Eds.). (2019). *Skin Aging & Cancer: Ambient UV-R Exposure*. Springer Singapore. https://doi.org/10.1007/978-981-13-2541-0

Edmondson, R., Broglie, J. J., Adcock, A. F., & Yang, L. (2014). Three-Dimensional Cell Culture Systems and Their Applications in Drug Discovery and Cell-Based Biosensors. *ASSAY and Drug Development Technologies*, *12*(4), 207–218. https://doi.org/10.1089/adt.2014.573

Elias, P. M. (2012). Structure and Function of the Stratum Corneum Extracellular Matrix. *Journal of Investigative Dermatology*, *132*(9), 2131–2133. https://doi.org/10.1038/jid.2012.246

Félétou, M. (2011). *The Endothelium: Part 1: Multiple Functions of the Endothelial Cells—Focus on Endothelium-Derived Vasoactive Mediators*. Morgan & Claypool Life Sciences. http://www.ncbi.nlm.nih.gov/books/NBK57149/

Fey, P. D., Saïd-Salim, B., Rupp, M. E., Hinrichs, S. H., Boxrud, D. J., Davis, C. C., Kreiswirth, B. N., & Schlievert, P. M. (2003). Comparative Molecular Analysis of Community- or Hospital-Acquired Methicillin-Resistant *Staphylococcus aureus*. *Antimicrobial Agents and Chemotherapy*, *47*(1), 196–203. https://doi.org/10.1128/AAC.47.1.196-203.2003

Ford, N. C., Benedeck, R. E., Mattoon, M. T., Peterson, J. K., Mesler, A. L., Veniaminova, N. A., Gardon, D. J., Tsai, S.-Y., Uchida, Y., & Wong, S. Y. (2024). Hair follicles modulate skin barrier function. *Cell Reports*, *43*(7), 114347. https://doi.org/10.1016/j.celrep.2024.114347

Foster, T. (1996). Staphylococcus. In S. Baron (Ed.), *Medical Microbiology* (4th ed.). University of Texas Medical Branch at Galveston. http://www.ncbi.nlm.nih.gov/books/NBK8448/

Fukuda, H., Sato, D., Iwamoto, T., Yamada, K., & Matsushita, K. (2020). Healthcare resources attributable to methicillin-resistant Staphylococcus aureus orthopedic surgical site infections. *Scientific Reports*, *10*(1), 17059. https://doi.org/10.1038/s41598-020-74070-4

Fukuda, K., Ito, Y., Furuichi, Y., Matsui, T., Horikawa, H., Miyano, T., Okada, T., Van Logtestijn, M., Tanaka, R. J., Miyawaki, A., & Amagai, M. (2024). Three stepwise pH progressions in stratum corneum for homeostatic maintenance of the skin. *Nature Communications*, *15*(1), 4062. https://doi.org/10.1038/s41467-024-48226-z

Funch, A. B., Mraz, V., Gadsbøll, A. Ø., Jee, M. H., Weber, J. F., Ødum, N., Woetmann, A., Johansen, J. D., Geisler, C., & Bonefeld, C. M. (2022). $CD8^+$ tissue-resident memory T cells recruit neutrophils that are essential for flare-ups in contact dermatitis. *Allergy*, *77*(2), 513–524. https://doi.org/10.1111/all.14986

Gangatirkar, P., Paquet-Fifield, S., Li, A., Rossi, R., & Kaur, P. (2007). Establishment of 3D organotypic cultures using human neonatal epidermal cells. *Nature Protocols*, *2*(1), 178–186. https://doi.org/10.1038/nprot.2006.448

Gao, C., Lu, C., Jian, Z., Zhang, T., Chen, Z., Zhu, Q., Tai, Z., & Liu, Y. (2021). 3D bioprinting for fabricating artificial skin tissue. *Colloids and Surfaces B: Biointerfaces*, *208*, 112041. https://doi.org/10.1016/j.colsurfb.2021.112041

Gray, C. (2025). Diabetic Foot Wound Heals With Early Detection And Care: A Complicated Case. *Wound Care Canada*. https://doi.org/10.56885/463546kiiead

Guo, X., & Che, W. (2024). Improvement of gram staining effect by ethanol pretreatment and quantization of staining image by unsupervised machine learning. *Archives of Microbiology*, *206*(7), 318. https://doi.org/10.1007/s00203-024-04045-w

Gurina, T. S., & Simms, L. (2025). Histology, Staining. In *StatPearls*. StatPearls Publishing. http://www.ncbi.nlm.nih.gov/books/NBK557663/

Heinrich, M. A., Liu, W., Jimenez, A., Yang, J., Akpek, A., Liu, X., Pi, Q., Mu, X., Hu, N., Schiffelers, R. M., Prakash, J., Xie, J., & Zhang, Y. S. (2019). 3D Bioprinting: From Benches to Translational Applications. *Small*, *15*(23), 1805510. https://doi.org/10.1002/smll.201805510

Hermsmeier, M., Jeong, S., Yamamoto, A., Chen, X., Nagavarapu, U., Evans, C. L., & Chan, K. F. (2018). Characterization of human cutaneous tissue autofluorescence: Implications in topical drug delivery studies with fluorescence microscopy. *Biomedical Optics Express*, *9*(11), 5400. https://doi.org/10.1364/BOE.9.005400

Holland, K. T., & Bojar, R. A. (2002). Cosmetics: What is Their Influence on the Skin Microflora? *American Journal of Clinical Dermatology*, *3*(7), 445–449. https://doi.org/10.2165/00128071-200203070-00001

Homepage—Eve Technologies. (2026). Retrieved February 2, 2026, from https://www.evetechnologies.com/

Iwase, T., Uehara, Y., Shinji, H., Tajima, A., Seo, H., Takada, K., Agata, T., & Mizunoe, Y. (2010). Staphylococcus epidermidis Esp inhibits Staphylococcus aureus biofilm formation and nasal colonization. *Nature*, *465*(7296), 346–349. https://doi.org/10.1038/nature09074

Javaeed, A., Qamar, S., Ali, S., Mustafa, M. A. T., Nusrat, A., & Ghauri, S. K. (2021). Histological Stains in the Past, Present, and Future. *Cureus*. https://doi.org/10.7759/cureus.18486

Kamel, M., Aleya, S., Alsubih, M., & Aleya, L. (2024). Microbiome Dynamics: A Paradigm Shift in Combatting Infectious Diseases. *Journal of Personalized Medicine*, *14*(2), 217. https://doi.org/10.3390/jpm14020217

Kathawala, M. H., Ng, W. L., Liu, D., Naing, M. W., Yeong, W. Y., Spiller, K. L., Van Dyke, M., & Ng, K. W. (2019). Healing of Chronic Wounds: An Update of Recent Developments and Future Possibilities. *Tissue Engineering. Part B, Reviews*, *25*(5), 429–444. https://doi.org/10.1089/ten.TEB.2019.0019

Keast, D., Wiesenfeld, L., Leblanc, K., & Landis, S. (2012). *CONNIE HARRIS RN ET IIWCC MSC*.

Kezic, S., O'Regan, G. M., Yau, N., Sandilands, A., Chen, H., Campbell, L. E., Kroboth, K., Watson, R., Rowland, M., Irwin McLean, W. H., & Irvine, A. D. (2011). Levels of filaggrin degradation products are influenced by both filaggrin genotype and atopic dermatitis severity. *Allergy*, *66*(7), 934–940. https://doi.org/10.1111/j.1398-9995.2010.02540.x

Kim, J. (2023). Characterization of Biocompatibility of Functional Bioinks for 3D Bioprinting. *Bioengineering*, *10*(4), 457. https://doi.org/10.3390/bioengineering10040457

Klechevsky, E., Morita, R., Liu, M., Cao, Y., Coquery, S., Thompson-Snipes, L., Briere, F., Chaussabel, D., Zurawski, G., Palucka, A. K., Reiter, Y., Banchereau, J., & Ueno, H. (2008). Functional Specializations of Human Epidermal Langerhans Cells and CD14+ Dermal Dendritic Cells. *Immunity*, *29*(3), 497–510. https://doi.org/10.1016/j.immuni.2008.07.013

Krieken, D., Ederveen, T., Hijum, S., Jansen, P., Melchers, W., Scheepers, P., Schalkwijk, J., & Zeeuwen, P. (2016). An In vitro Model for Bacterial Growth on Human Stratum Corneum. *Acta Dermato Venereologica*, *96*(7), 873–879. https://doi.org/10.2340/00015555-2401

Kuhnke, J. L., Burrows, C., Evans, R., Orsted, H., & Rosenthal, S. (2024). Best Practice Recommendations For Skin Health And Wound Management 2025. In *Best Practice*

Recommendations For Skin Health and Wound Management 2024 (pp. 1–3). Wounds Canada. https://doi.org/10.56885/HXLA9381

Le, V. H., King, T., Wuerzberger, B., Bauer, O. R., Carver, M. N., Chan, T. S., Henson, A. L., Hubbard, G. K., Kopadze, T., Patterson, C. F., McGraw, S. M., O'Hara, A., Yarkosky, E. J., LaMontagne, M. G., Hotze, E. M., & Ferreira, R. B. R. (2025). Metabolites derived from bacterial isolates of the human skin microbiome inhibit *Staphylococcus aureus* biofilm formation. *Microbiology Spectrum*, *13*(9), e01306-25. https://doi.org/10.1128/spectrum.01306-25

Lee, D. H., Oh, J.-H., & Chung, J. H. (2016). Glycosaminoglycan and proteoglycan in skin aging. *Journal of Dermatological Science*, *83*(3), 174–181. https://doi.org/10.1016/j.jdermsci.2016.05.016

Lee, H.-J., & Kim, M. (2022). Skin Barrier Function and the Microbiome. *International Journal of Molecular Sciences*, *23*(21), 13071. https://doi.org/10.3390/ijms232113071

Liu, Q., Ranallo, R., Rios, C., Grice, E. A., Moon, K., & Gallo, R. L. (2023). Crosstalk between skin microbiota and immune system in health and disease. *Nature Immunology*, *24*(6), 895–898. https://doi.org/10.1038/s41590-023-01500-6

Liu, R., Feng, J., Ni, Y., Chen, K., Wang, Y., Zhang, T., Zhou, M., & Zhao, C. (2024). Dysbiosis and diabetic foot ulcers: A metabolic perspective of Staphylococcus aureus infection. *Biomedicine & Pharmacotherapy*, *180*, 117498. https://doi.org/10.1016/j.biopha.2024.117498

Lopez-Ojeda, W., Pandey, A., Alhajj, M., & Oakley, A. M. (2025). Anatomy, Skin (Integument). In *StatPearls*. StatPearls Publishing. http://www.ncbi.nlm.nih.gov/books/NBK441980/

Madison, K. C., Swartzendruber, D. C., Wertz, P. W., & Downing, D. T. (1988). Lamellar Granule Extrusion and Stratum Corneum Intercellular Lamellae in Murine Keratinocyte Cultures. *Journal of Investigative Dermatology*, *90*(2), 110–116. https://doi.org/10.1111/1523-1747.ep12462065

Maksimoska, V., Dan, Q., Rambharack, N., & Szászi, K. (2025). Keratinocyte-derived VEGF-A is an essential pro-migratory autocrine mediator, acting through the KDR/GEF-H1/RhoA pathway. *Frontiers in Cell and Developmental Biology*, *13*, 1601887. https://doi.org/10.3389/fcell.2025.1601887

Mamun, A. A., Shao, C., Geng, P., Wang, S., & Xiao, J. (2024). Recent advances in molecular mechanisms of skin wound healing and its treatments. *Frontiers in Immunology*, *15*, 1395479. https://doi.org/10.3389/fimmu.2024.1395479

Matsui, T., & Amagai, M. (2015). Dissecting the formation, structure and barrier function of the stratum corneum. *International Immunology*, *27*(6), 269–280. https://doi.org/10.1093/intimm/dxv013

Morán, G. A. G., Parra-Medina, R., Cardona, A. G., Quintero-Ronderos, P., & Rodríguez, É. G. (2013). Cytokines, chemokines and growth factors. In *Autoimmunity: From Bench to Bedside [Internet]*. El Rosario University Press. https://www.ncbi.nlm.nih.gov/books/NBK459450/

Nair, N., Biswas, R., Götz, F., & Biswas, L. (2014). Impact of Staphylococcus aureus on Pathogenesis in Polymicrobial Infections. *Infection and Immunity*, *82*(6), 2162–2169. https://doi.org/10.1128/IAI.00059-14

Neagu, M., Constantin, C., Jugulete, G., Cauni, V., Dubrac, S., Szöllősi, A. G., & Zurac, S. (2022). Langerhans Cells—Revising Their Role in Skin Pathologies. *Journal of Personalized Medicine*, *12*(12), 2072. https://doi.org/10.3390/jpm12122072

Ouyang, L., Yao, R., Chen, X., Na, J., & Sun, W. (2015). 3D printing of HEK 293FT cell-laden hydrogel into macroporous constructs with high cell viability and normal biological functions. *Biofabrication*, *7*(1), 015010. https://doi.org/10.1088/1758-5090/7/1/015010

Pal, S., Sayana, A., Joshi, A., & Juyal, D. (2019). Staphylococcus aureus: A predominant cause of surgical site infections in a rural healthcare setup of Uttarakhand. *Journal of Family Medicine and Primary Care*, *8*(11), 3600. https://doi.org/10.4103/jfmpc.jfmpc_521_19

Patra, V., Laoubi, L., Nicolas, J.-F., Vocanson, M., & Wolf, P. (2018). A Perspective on the Interplay of Ultraviolet-Radiation, Skin Microbiome and Skin Resident Memory TCRαβ+ Cells. *Frontiers in Medicine*, *5*, 166. https://doi.org/10.3389/fmed.2018.00166

Pazhouhnia, Z., Noori, A., Farzin, A., Khoshmaram, K., Hoseinpour, M., Ai, J., Ebrahimi, M., & Lotfibakhshaiesh, N. (2024). 3D-bioprinted GelMA/gelatin/amniotic membrane extract (AME) scaffold loaded with keratinocytes, fibroblasts, and endothelial cells for skin tissue engineering. *Scientific Reports*, *14*(1), 12670. https://doi.org/10.1038/s41598-024-62926-y

Peña, O. A., & Martin, P. (2024). Cellular and molecular mechanisms of skin wound healing. *Nature Reviews Molecular Cell Biology*, *25*(8), 599–616. https://doi.org/10.1038/s41580-024-00715-1

Pérez-Panero, A. J., Ruiz-Muñoz, M., Cuesta-Vargas, A. I., & Gónzalez-Sánchez, M. (2019). Prevention, assessment, diagnosis and management of diabetic foot based on clinical practice guidelines: A systematic review. *Medicine*, *98*(35), e16877. https://doi.org/10.1097/MD.0000000000016877

Pfisterer, K., Shaw, L. E., Symmank, D., & Weninger, W. (2021). The Extracellular Matrix in Skin Inflammation and Infection. *Frontiers in Cell and Developmental Biology*, *9*, 682414. https://doi.org/10.3389/fcell.2021.682414

Prism_v5_Statistics_Guide. (2007).

Prost-squarcioni, C., Fraitag, S., Heller, M., & Boehm, N. (2008). Histologie fonctionnelle du derme. *Annales de Dermatologie et de Vénéréologie*, *135*(1), 5–20. https://doi.org/10.1016/S0151-9638(08)70206-0

Purkerson, J., Colon, L., Poole, C., Corbett, A., & Pryhuber, G. S. (2023). *801.1.HTC_H&E Stain (Paraffin or Cryosections)*. https://www.protocols.io/view/801-1-htc-h-amp-e-stain-paraffin-or-cryosections-c6iyzcfw

Ragauskas, T., Uzieliene, I., & Bernotiene, E. (2025). Histological Processing of Scaffolds: Challenges and Solutions. *Journal of Functional Biomaterials*, *16*(8), 279. https://doi.org/10.3390/jfb16080279

Raziyeva, K., Kim, Y., Zharkinbekov, Z., Kassymbek, K., Jimi, S., & Saparov, A. (2021). Immunology of Acute and Chronic Wound Healing. *Biomolecules*, *11*(5), 700. https://doi.org/10.3390/biom11050700

Restan Perez, M., Masri, N., Walters-Shumka, J., Kahale, S., & Willerth, S. (2023). Protocol for 3D Bioprinting Mesenchymal Stem Cell–derived Neural Tissues Using a Fibrin-based Bioink. *BIO-PROTOCOL*, *13*(9). https://doi.org/10.21769/BioProtoc.4663

Rielland, M., Bernerd, F., Camman, M., Tan, X., & Seyler, N. (2025). Development of pathological skin models: From conventional techniques to 3D bioprinting. *Frontiers in Bioengineering and Biotechnology*, *13*, 1538774. https://doi.org/10.3389/fbioe.2025.1538774

Rossi, A., Pescara, T., Gambelli, A. M., Gaggia, F., Asthana, A., Perrier, Q., Basta, G., Moretti, M., Senin, N., Rossi, F., Orlando, G., & Calafiore, R. (2024). Biomaterials for extrusion-based bioprinting and biomedical applications. *Frontiers in Bioengineering and Biotechnology*, *12*, 1393641. https://doi.org/10.3389/fbioe.2024.1393641

Round, J. L., & Mazmanian, S. K. (2010). Inducible Foxp3$^+$ regulatory T-cell development by a commensal bacterium of the intestinal microbiota. *Proceedings of the National Academy of Sciences*, *107*(27), 12204–12209. https://doi.org/10.1073/pnas.0909122107

Ruan, J.-L., Tulloch, N. L., Muskheli, V., Genova, E. E., Mariner, P. D., Anseth, K. S., & Murry, C. E. (2013). An Improved Cryosection Method for Polyethylene Glycol Hydrogels Used in Tissue Engineering. *Tissue Engineering Part C: Methods*, *19*(10), 794–801. https://doi.org/10.1089/ten.tec.2012.0460

Satapathy, T., Yadu, H., & Sahu, P. (2025). Protective Role of Herbal Bioactive in Modulation of PDGF-VEGF-TGFβ-EGF Fibroblast Proliferation and Re-epithelialization for the Enhancement of Tissue Strength and Wound Healing. *Regenerative Engineering and Translational Medicine*. https://doi.org/10.1007/s40883-025-00495-w

Schreml, S., Szeimies, R. M., Prantl, L., Karrer, S., Landthaler, M., & Babilas, P. (2010). Oxygen in acute and chronic wound healing: Oxygen in wound healing. *British Journal of Dermatology*, *163*(2), 257–268. https://doi.org/10.1111/j.1365-2133.2010.09804.x

Schultz, G. S., Chin, G. A., Moldawer, L., & Diegelmann, R. F. (2011). Principles of Wound Healing. In R. Fitridge & M. Thompson (Eds.), *Mechanisms of Vascular Disease: A Reference Book for Vascular Specialists*. University of Adelaide Press. http://www.ncbi.nlm.nih.gov/books/NBK534261/

Sell, S. A., Wolfe, P. S., Garg, K., McCool, J. M., Rodriguez, I. A., & Bowlin, G. L. (2010). The Use of Natural Polymers in Tissue Engineering: A Focus on Electrospun Extracellular Matrix Analogues. *Polymers*, *2*(4), 522–553. https://doi.org/10.3390/polym2040522

Shai, A., & Maibach, H. I. (Eds.). (2005). *Wound Healing and Ulcers of the Skin: Diagnosis and Therapy — The Practical Approach*. Springer-Verlag Berlin Heidelberg. https://doi.org/10.1007/b138035

Shi, H., Li, Y., Xu, K., & Yin, J. (2023). Advantages of photo-curable collagen-based cell-laden bioinks compared to methacrylated gelatin (GelMA) in digital light processing (DLP) and

extrusion bioprinting. *Materials Today Bio*, *23*, 100799. https://doi.org/10.1016/j.mtbio.2023.100799

Sim, P., Strudwick, X. L., Song, Y., Cowin, A. J., & Garg, S. (2022). Influence of Acidic pH on Wound Healing In Vivo: A Novel Perspective for Wound Treatment. *International Journal of Molecular Sciences*, *23*(21), 13655. https://doi.org/10.3390/ijms232113655

Smith gram staining. (2016).

Stefanovic, N., & Irvine, A. D. (2024). Filaggrin and beyond. *Annals of Allergy, Asthma & Immunology*, *132*(2), 187–195. https://doi.org/10.1016/j.anai.2023.09.009

Stepanovska, J., Supova, M., Hanzalek, K., Broz, A., & Matejka, R. (2021). Collagen Bioinks for Bioprinting: A Systematic Review of Hydrogel Properties, Bioprinting Parameters, Protocols, and Bioprinted Structure Characteristics. *Biomedicines*, *9*(9), 1137. https://doi.org/10.3390/biomedicines9091137

Šuler Baglama, Š., & Trčko, K. (2022). Skin and gut microbiota dysbiosis in autoimmune and inflammatory skin diseases. *Acta Dermatovenerologica Alpina Pannonica et Adriatica*, *31*(3). https://doi.org/10.15570/actaapa.2022.16

Sun, X., Ren, W., Xie, L., Ren, Q., Zhu, Z., Jia, Q., Jiang, W., Jin, Z., & Yu, Y. (2024). Recent advances in 3D bioprinting of tissues and organs for transplantation and drug screening. *Virtual and Physical Prototyping*, *19*(1), e2384662. https://doi.org/10.1080/17452759.2024.2384662

Thomas, S., Liu, W., Arora, S., Ganesh, V., Ko, Y.-P., & Höök, M. (2019). The Complex Fibrinogen Interactions of the Staphylococcus aureus Coagulases. *Frontiers in Cellular and Infection Microbiology*, *9*, 106. https://doi.org/10.3389/fcimb.2019.00106

Tito, C., Masciarelli, S., Colotti, G., & Fazi, F. (2025). EGF receptor in organ development, tissue homeostasis and regeneration. *Journal of Biomedical Science*, *32*(1), 24. https://doi.org/10.1186/s12929-025-01119-9

Tripathi, S., Mandal, S. S., Bauri, S., & Maiti, P. (2023). 3D bioprinting and its innovative approach for biomedical applications. *MedComm*, *4*(1), e194. https://doi.org/10.1002/mco2.194

Usui, M. L., Mansbridge, J. N., Carter, W. G., Fujita, M., & Olerud, J. E. (2008). Keratinocyte Migration, Proliferation, and Differentiation in Chronic Ulcers From Patients With

Diabetes and Normal Wounds. *Journal of Histochemistry & Cytochemistry*, *56*(7), 687–696. https://doi.org/10.1369/jhc.2008.951194

Varpe, A., Sayed, M., & Mane, N. S. (2025). A Comprehensive Literature Review on Advancements and Challenges in 3D Bioprinting of Human Organs: Ear, Skin, and Bone. *Annals of Biomedical Engineering*, *53*(1), 14–33. https://doi.org/10.1007/s10439-024-03580-3

Volksdorf, T., & Brandner, J. M. (2018). Tight Junctions and Cutaneous Wound Healing. In *Wound Healing* (pp. 31–42). John Wiley & Sons, Ltd. https://doi.org/10.1002/9781119282518.ch3

Wang, P., Li, H., Zhang, Xingjiang, Wang, X., Sun, W., Zhang, Xiaoya, Chi, B., Go, Y., Chan, X. H. F., Wu, J., & Huang, Q. (2025). Microecology in vitro model replicates the human skin microbiome interactions. *Nature Communications*, *16*(1), 3085. https://doi.org/10.1038/s41467-025-58377-2

Wang, X., Ao, Q., Tian, X., Fan, J., Tong, H., Hou, W., & Bai, S. (2017). Gelatin-Based Hydrogels for Organ 3D Bioprinting. *Polymers*, *9*(9), 401. https://doi.org/10.3390/polym9090401

Weng, T., Zhang, W., Xia, Y., Wu, P., Yang, M., Jin, R., Xia, S., Wang, J., You, C., Han, C., & Wang, X. (2021). 3D bioprinting for skin tissue engineering: Current status and perspectives. *Journal of Tissue Engineering*, *12*, 20417314211028574. https://doi.org/10.1177/20417314211028574

Werner, S., & Grose, R. (2003). Regulation of Wound Healing by Growth Factors and Cytokines. *Physiological Reviews*, *83*(3), 835–870. https://doi.org/10.1152/physrev.2003.83.3.835

Whiteside, T. L. (2002). Cytokine Assays. *BioTechniques*, *33*(sup4), 1. https://doi.org/10.2144/Oct0202

Wilgus, T. A., & Wulff, B. C. (2014). The Importance of Mast Cells in Dermal Scarring. *Advances in Wound Care*, *3*(4), 356–365. https://doi.org/10.1089/wound.2013.0457

Xu, H.-Q., Liu, J.-C., Zhang, Z.-Y., & Xu, C.-X. (2022). A review on cell damage, viability, and functionality during 3D bioprinting. *Military Medical Research*, *9*(1), 70. https://doi.org/10.1186/s40779-022-00429-5

Yousef, H., Alhajj, M., Fakoya, A. O., & Sharma, S. (2025). Anatomy, Skin (Integument), Epidermis. In *StatPearls*. StatPearls Publishing. http://www.ncbi.nlm.nih.gov/books/NBK470464/

Zhang, X.-E., Zheng, P., Ye, S.-Z., Ma, X., Liu, E., Pang, Y.-B., He, Q.-Y., Zhang, Y.-X., Li, W.-Q., Zeng, J.-H., & Guo, J. (2024). Microbiome: Role in Inflammatory Skin Diseases. *Journal of Inflammation Research*, *Volume 17*, 1057–1082. https://doi.org/10.2147/JIR.S441100

Zhang, Y., Seminario-Vidal, L., Cohen, L., Hussaini, M., Yao, J., Rutenberg, D., Kim, Y., Giualiano, A., Robinson, L. A., & Sokol, L. (2022). "Alterations in the Skin Microbiota Are Associated With Symptom Severity in Mycosis Fungoides." *Frontiers in Cellular and Infection Microbiology*, *12*, 850509. https://doi.org/10.3389/fcimb.2022.850509

Zheng, S. G. (2013). *Regulatory T cells vs Th17: Differentiation of Th17 versus Treg, are the mutually exclusive?*

Zheng, Y., Hunt, R. L., Villaruz, A. E., Fisher, E. L., Liu, R., Liu, Q., Cheung, G. Y. C., Li, M., & Otto, M. (2022). Commensal Staphylococcus epidermidis contributes to skin barrier homeostasis by generating protective ceramides. *Cell Host & Microbe*, *30*(3), 301-313.e9. https://doi.org/10.1016/j.chom.2022.01.004

Zhou, R., & Mei, L. (Eds.). (2013). *Neural Development: Methods and Protocols* (Vol. 1018). Humana Press. https://doi.org/10.1007/978-1-62703-444-9